Jackson, M. G., Becker, T. W., Steinberger, B. (2021): Spatial Characteristics of Recycled and Primordial Reservoirs in the Deep Mantle. - Geochemistry Geophysics Geosystems (G3), 22, 3, e2020GC009525.

https://doi.org/10.1029/2020GC009525

Geochemistry, Geophysics, Geosystems

RESEARCH ARTICLE
10.1029/2020GC009525

Key Points:

- High-^{3}He/^{4}He signatures at hotspots are not confined to the Large Low Shear Wave Velocity Provinces (LLSVPs), because the high-^{3}He/^{4}He Yellowstone hotspot is not linked to the LLSVPs
- Plume dynamics (i.e., buoyancy), not geography, determines whether a deep, dense, and possibly widespread high-^{3}He/^{4}He domain is entrained
- Plume-fed EM (enriched mantle) hotspots are associated with the southern regions of both LLSVPs; HIMU hotspots are not linked to the LLSVPs

Supporting Information:

- Supporting Information S1
- Figures S1-S6
- Tables S1-S3

Correspondence to:
M. G. Jackson,
jackson@geol.ucsb.edu

Citation:
Jackson, M. G., Becker, T. W., & Steinberger, B. (2021). Spatial characteristics of recycled and primordial reservoirs in the deep mantle. *Geochemistry, Geophysics, Geosystems*, *22*, e2020GC009525. https://doi.org/10.1029/2020GC009525

Received 9 NOV 2020
Accepted 10 JAN 2021

Spatial Characteristics of Recycled and Primordial Reservoirs in the Deep Mantle

M. G. Jackson[1], T. W. Becker[2], and B. Steinberger[3,4]

[1]Department of Earth Science, University of California, Santa Barbara, Santa Barbara, CA, USA, [2]Department of Geological Sciences, Institute for Geophysics, Jackson School of Geosciences, The University of Texas at Austin, Austin, TX, USA, [3]Section 2.5 Geodynamic Modelling, GFZ German Research Centre for Geosciences, Potsdam, Germany, [4]Centre for Earth Evolution and Dynamics, University of Oslo, Oslo, Norway

Abstract The spatial distribution of the geochemical domains hosting recycled crust and primordial (high-^{3}He/^{4}He) reservoirs, and how they are linked to mantle convection, are poorly understood. Two continent-sized seismic anomalies located near the core-mantle boundary—called the Large Low Shear Wave Velocity Provinces (LLSVPs)—are potential geochemical reservoir hosts. It has been suggested that high-^{3}He/^{4}He hotspots are spatially confined to the LLSVPs, hotspots sampling recycled continental crust are associated with only one of the LLSVPs, and recycled continental crust shows no relationship with latitude. We reevaluate the links between LLSVPs and isotopic signatures of hotspot lavas using improved mantle flow models including plume conduit advection. While most hotspots with the highest-^{3}He/^{4}He can indeed be traced to the LLSVP interiors, at least one high-^{3}He/^{4}He hotspot, Yellowstone, is located outside of the LLSVPs. This suggests high-^{3}He/^{4}He is not geographically confined to the LLSVPs. Instead, a positive correlation between hotspot buoyancy flux and maximum hotspot ^{3}He/^{4}He suggests that it is plume dynamics (i.e., buoyancy), not geography, which determines whether a dense, deep, and possibly widespread high-^{3}He/^{4}He reservoir is entrained. We also show that plume-fed EM hotspots (enriched mantle, with low-^{143}Nd/^{144}Nd), signaling recycled continental crust, are spatially linked to both LLSVPs, and located primarily in the southern hemisphere. Lastly, we confirm that hotspots sampling HIMU ("high-μ," or high ^{238}U/^{204}Pb) domains are not spatially limited to the LLSVPs. These findings clarify and advance our understanding of deep mantle reservoir distributions, and we discuss how continental and oceanic crust subduction is consistent with the spatial decoupling of EM and HIMU.

1. Introduction

Hotspot volcanoes erupt lavas that are melts of buoyantly upwelling mantle plumes from the deep mantle. The radiogenic isotopic compositions (^{3}He/^{4}He, ^{143}Nd/^{144}Nd, ^{206}Pb/^{204}Pb, etc.) of hotspot lavas, which are unchanged by mantle melting processes, thus provide windows into the chemical make-up of the inaccessibly deep mantle sourced by plumes. A primary observation made from the geochemical characterization of hotspot lavas is that the mantle entrained by upwelling plumes is heterogeneous and contains primordial isotopic signatures, including high ^{3}He/^{4}He ratios. However, hotspot lavas also record signatures of subducted oceanic and continental crust recycled back to the near-surface from ancient subduction zones (Hofmann & White, 1982; White & Hofmann, 1982) that are associated with low ^{3}He/^{4}He (e.g., Hanyu & Kaneoka, 1997; Jackson et al., 2007a; Kurz et al., 1982). Thus, both recycled and primordial domains exist in the mantle sources of upwelling plumes, but the spatial relationships among these reservoirs are poorly understood.

Mantle reservoirs hosting subducted crust have unique isotopic fingerprints that reflect timescales since formation and subduction as well as the processes that acted on the rock protoliths prior to, during, and following subduction. There are many proposed models for the origin of hotspot lavas with HIMU ("high-μ," or high ^{238}U/^{204}Pb) signatures (e.g., Castillo, 2015; Castillo et al., 2018; Eisele et al., 2002; Kendrick et al., 2017; Pilet et al., 2008; Weiss et al., 2016), characterized by having high ^{206}Pb/^{204}Pb, low ^{3}He/^{4}He (<8 Ra), and long-term incompatible element depletion resulting in high ^{143}Nd/^{144}Nd (referred to as geochemically depleted ^{143}Nd/^{144}Nd compositions). Nonetheless, a common interpretation of the HIMU geochemical signature is that it arises from recycled oceanic crust (Hofmann & White, 1982). Similarly, ancient recycled continental

crust and associated sediments evolve into EM (enriched mantle) reservoirs (White & Hofmann, 1982) that exhibit geochemically enriched (low) $^{143}Nd/^{144}Nd$ and low $^{3}He/^{4}He$.

In contrast, mantle domains with primordial high $^{3}He/^{4}He$ (up to ~50 Ra) (Starkey et al., 2009) signatures are characterized by geochemically depleted (high) $^{143}Nd/^{144}Nd$ ratios and low $^{206}Pb/^{204}Pb$. Mantle domains with primordial $^{3}He/^{4}He$ have also been associated with anomalous ^{129}Xe (Mukhopadhyay, 2012), ^{182}W (Mundl et al., 2017; Mundl-Petermeier et al., 2020; Rizo et al., 2019), and ^{142}Nd (Horan et al., 2018; Peters et al., 2018) isotopic compositions, which are the products of short-lived nuclides extant only in the Hadean: ^{129}I (half-life $T_{1/2}$ = 15.7 Ma), ^{182}Hf ($T_{1/2}$ = 8.9 Ma), and ^{146}Sm ($T_{1/2}$ = 103 Ma), respectively. These observations support an early Hadean origin of the high $^{3}He/^{4}He$ domain followed by long-term preservation in the mantle. However, it is not known how anomalies generated in the Hadean survived ~4.5 Ga of mantle convection to be sampled by modern basalts. The viscosity and density of the host reservoirs will control mixing (e.g., Ballmer et al., 2017; Becker et al., 1999; Davaille, 1999; McNamara & Zhong, 2004), and reservoir preservation may also relate to where these primordial domains reside, thereby providing constraints on dynamics (e.g., Coltice et al., 2005; Dechamps et al., 2011; Jackson et al., 2017; Lin & van Keken, 2006; Samuel & Farnetani, 2003). Thus, it is critical to better constrain where primordial, and recycled, domains are stored in the Earth's mantle.

In contrast to the depleted mantle (DM)—which has geochemically depleted $^{143}Nd/^{144}Nd$, low $^{206}Pb/^{204}Pb$, and low $^{3}He/^{4}He$, and is sampled from the upper mantle by mid-ocean ridge basalts (MORB; Gale et al., 2013)—high-$^{3}He/^{4}He$ signatures are relatively rare and are sampled only by hotspots fed by the hottest plumes with the highest buoyancy fluxes, supporting a deep-mantle origin for a high-$^{3}He/^{4}He$ mantle domain that is relatively dense (Jackson et al., 2017). In addition, hotspots that erupt extreme EM or HIMU components tend to be associated with seismically resolved mantle plumes (Jackson et al., 2018a), which supports a deep mantle home for recycled crust sampled by plumes. However, the spatial relationships between primordial (high $^{3}He/^{4}He$) and recycled (EM and HIMU) domains in the deep mantle are not well known. The two near-antipodal, deep mantle LLSVPs (large low shear wave velocity provinces)—one LLSVP located under the Pacific Ocean, and the other LLSVP situated under Africa and the Atlantic and Indian Oceans, called the Indo-Atlantic LLSVP hereafter—are attractive in this regard, but studies suggesting they are home to primordial and recycled domains yield conflicting conclusions.

Williams et al. (2019) explored laterally advected plume conduits where, instead of rising vertically, conduits tilt in the “mantle wind” (Boschi et al., 2007; Steinberger & O'Connell, 1998). Williams et al. (2019) traced high-$^{3}He/^{4}He$ hotspot associated plumes and concluded that the high $^{3}He/^{4}He$ source region is restricted to the LLSVPs. However, that study excluded Yellowstone, which is a high $^{3}He/^{4}He$ hotspot with a likely deep source underneath the Americas (Nelson & Grand, 2018; Steinberger et al., 2019), suggesting high $^{3}He/^{4}He$ material is in fact not restricted to the LLSVPs.

While arguing for a connection between high $^{3}He/^{4}He$ and the LLSVPs, Williams et al. (2019) rejected a geographic relationship between LLSVPs and conduits sourcing hotspots that exhibit recycled crust signatures (Williams et al., 2019), where recycled crust signatures were defined by having the maximum $^{208}Pb^{*}/^{206}Pb^{*}$ at each hotspot (where $^{208}Pb^{*}/^{206}Pb^{*} = (^{208}Pb/^{204}Pb–29.475)/(^{206}Pb/^{204}Pb – 9.306)$) (Galer & O'Nions, 1985). In contrast, Castillo (1988) and Jackson et al. (2018b) showed that hotspots with EM signatures, associated with continental crust recycling, are geographically restricted to both the Indo-Atlantic and Pacific LLSVPs, but these studies did not explore whether primordial high $^{3}He/^{4}He$ is also associated with the LLSVPs. Another potential weakness of those studies is that they assumed vertical, instead of advected, plume conduits, for simplicity. In addition, Jackson et al. (2018b) showed that, while EM reservoirs do appear to be geographically restricted to the LLSVPs, HIMU domains are not.

More recently, Doucet et al. (2020) arrived at two unexpected conclusions regarding the distribution of EM hotspots: (1) deeply sourced plumes with EM signatures are linked only with the Indo-Atlantic and not the Pacific LLSVP, and (2) the distribution of the EM domain is not related to latitude. Doucet et al. (2020) excluded geochemical data for hotspots with seismically resolved plumes that did not meet specific criteria. Partially because of this filtering, Doucet et al.'s (2020) results contrast with the proposed geographic association between EM hotspots and *both* the Indo-Atlantic and Pacific LLSVPs (Castillo, 1988; Jackson et al., 2018b). Doucet et al. (2020) also rejected the suggestion that EM domains are concentrated in a

large-scale southern hemispheric geochemical province referred to as the DUPAL anomaly (*Dup*ré+*Al*lègre from Dupré & Allègre, 1983; Hart, 1984).

Therefore, key questions regarding the distribution of recycled and primordial domains in the deep Earth remain (Doucet et al., 2020; Jackson et al., 2018b; Konter & Becker, 2012; William et al., 2019). Are primordial or recycled domains, or both, located in the LLSVPs? Does just one LLSVP exhibit clear signatures of recycled continental crust, or do both? Given that the protoliths for recycled mantle reservoirs—continental and oceanic crust—are likely subducted together, with similar trajectories governed by large-scale subduction associated transport, why are EM and HIMU domains seemingly spatially decoupled in the mantle? Do geochemical reservoirs exhibit geographic distributions that favor one hemisphere over the other, or is a hemisphere-scale DUPAL domain an outdated concept?

The answers to these questions bear on the thermo-chemical convection dynamics that control the co-evolution of the surface and deep mantle over geologic time, including mechanisms for the long-term preservation of geochemical domains and processes that influence their geographic distribution in the deep Earth.

2. Methods

We address these questions by comparing the inferred geographic distributions of the lower mantle sources of 58 hotspots with geochemical signatures that trace primordial and recycled material measured in hotspot lavas (Figure 1). Our geochemical database seeks to represent the most geochemically extreme lavas from each hotspot to identify the global distribution of EM, HIMU, and high $^{3}He/^{4}He$ lavas. Values for the highest $^{3}He/^{4}He$ (most primordial), lowest $^{143}Nd/^{144}Nd$ (useful for identifying the strongest EM signatures), and highest $^{206}Pb/^{204}Pb$ (for identifying the strongest HIMU signatures) lavas at each hotspot are provided in Table S1. In most cases, the geochemically extreme compositions at any given hotspot are measured on different lavas, but there are several exceptions where the lowest $^{143}Nd/^{144}Nd$ and highest $^{206}Pb/^{204}Pb$ at a given hotspot are found in a single lava (Jackson et al., 2018a, 2018b). We define elevated $^{3}He/^{4}He$ as being higher than the $^{3}He/^{4}He$ range for global MORB away from hotspots (8 ± 2 Ra, 2σ; Graham, 2002). In addition, high $^{206}Pb/^{204}Pb$ (HIMU) hotspots have at least one lava with $^{206}Pb/^{204}Pb \geq 20$ (a threshold defined and justified in Jackson et al., 2018b), and $^{143}Nd/^{144}Nd$ value is not considered in defining whether hotspots have HIMU compositions. Geochemically enriched (EM) hotspots have at least one lava with $^{143}Nd/^{144}Nd \leq 0.512630$ (where 0.512630 is the chondritic $^{143}Nd/^{144}Nd$ value; Bouvier et al., 2008), and $^{206}Pb/^{204}Pb$ values are not considered in defining whether hotspots have EM compositions. Mantle domains with $^{143}Nd/^{144}Nd > 0.512630$ have experienced past melt extraction and depletion of highly incompatible relative to less incompatible elements, and are considered to be incompatible element depleted (or, more simply, geochemically depleted). In contrast, mantle domains with $^{143}Nd/^{144}Nd < 0.512630$ have experience incompatible element addition, and such mantle domains are referred to as incompatible element enriched, or geochemically enriched.

We also provide new $^{3}He/^{4}He$ data for the San Felix hotspot, a hotspot that has never been characterized for $^{3}He/^{4}He$ (Table S2). Analytical methods for $^{3}He/^{4}He$ measurement are provided in the supporting information Text S1.

Continental lithosphere assimilation at continental hotspots will decrease $^{3}He/^{4}He$ ratios, so measured $^{3}He/^{4}He$ data at continental hotspots are treated as minima. Therefore, figures that include $^{3}He/^{4}He$ show oceanic and continental hotspots separately. In contrast, the impact of continental assimilation on $^{143}Nd/^{144}Nd$, and especially $^{206}Pb/^{204}Pb$, is less predictable. Thus, Nd and Pb isotopic systematics at continental hotspot lavas are not evaluated here.

To assess ensemble uncertainties for Earth structure and inferred dynamic models, we use four global seismic tomography models—S40RTS (Ritsema et al., 2011), SEMUCB-WM1 (French & Romanowicz, 2015), the composite SMEAN2 (Becker & Boschi, 2002; Jackson et al., 2017), and TX2016 (Lu & Grand, 2016)—in an internally consistent way to, (1), evaluate how plumes tilt in mantle flow as they upwell, (2), define mantle plume conduits beneath hotspots, and, (3), delineate the margins of the LLSVPs.

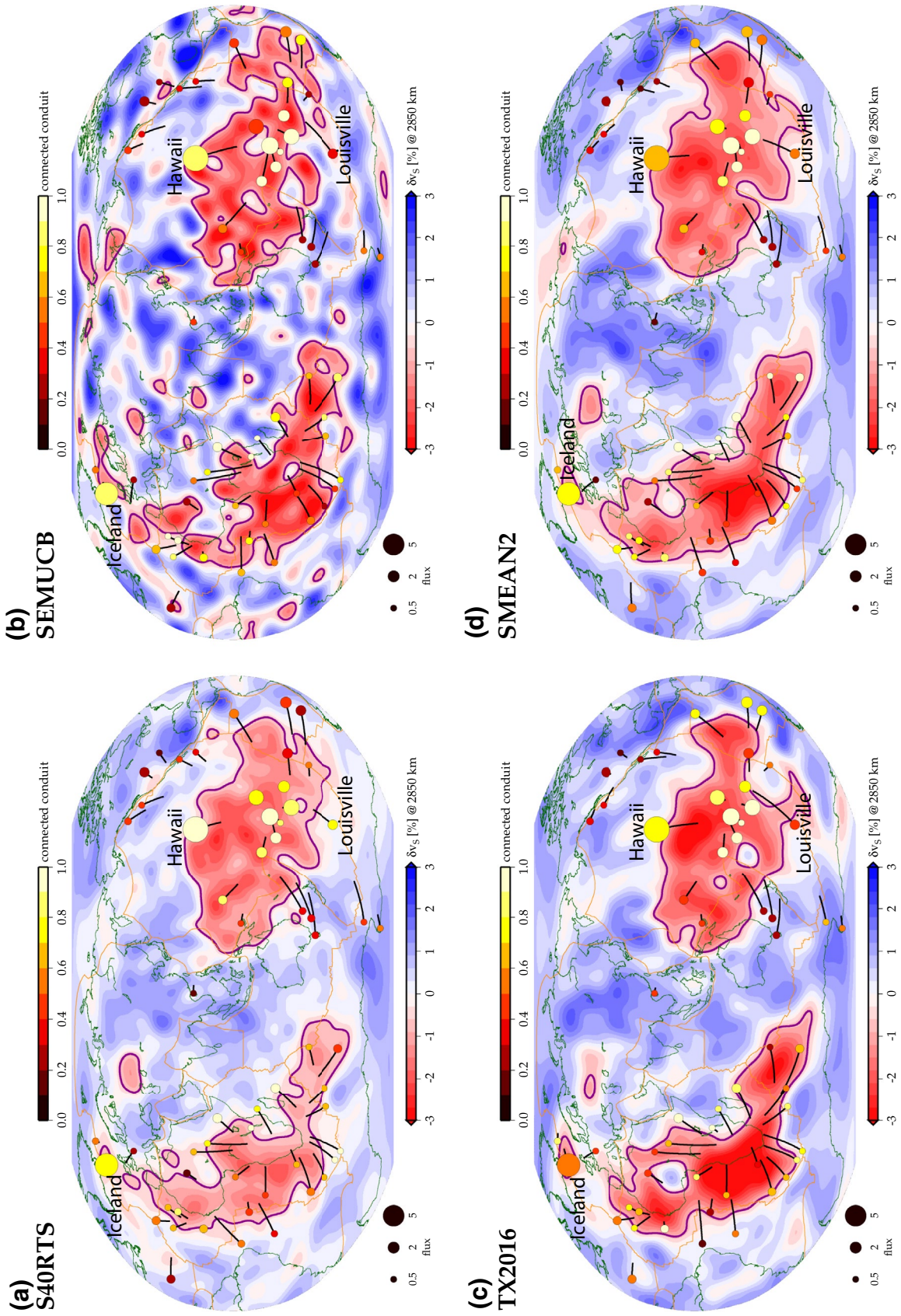
(a)
S40RTS
(b)
SEMUCB
(c)
TX2016
(d)
SMEAN2
Hawaii
Louisville
Iceland
connected conduit
0.0
0.2
0.4
0.6
0.8
1.0
δvS [%] @ 2850 km
-3
-2
-1
0
1
2
3
flux
0.5
2
5

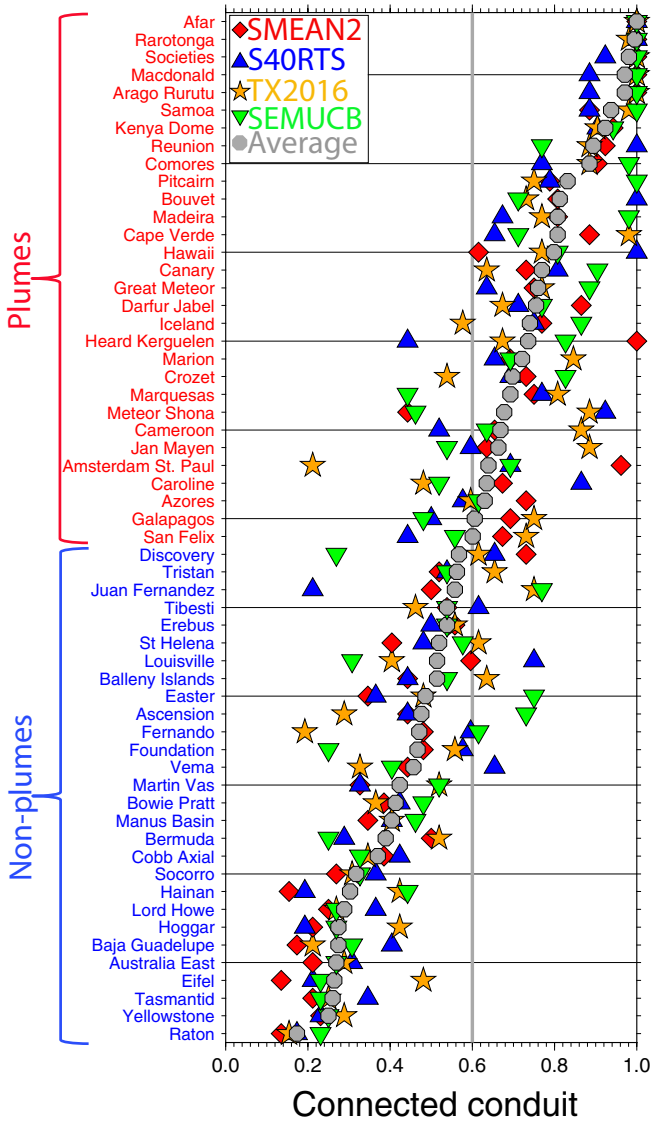

Figure 2. Distribution of normalized connected conduit lengths for different tomographic models (cf. Boschi et al., 2007) for all hotspots. The connected conduit value is the fraction of each modeled hotspot's associated plume conduit that is located in slow tomographic velocity anomalies (Text S1 in the supporting information). The connected conduit lengths for individual seismic models are shown with different color symbols, and the average conduit length across the four seismic models is also shown (gray). The latter is used to define whether a hotspot is associated with a plume. If the connected conduit is ≥ 0.6 (where 0.6 is approximately the average connected conduit length for the tomographic models), the associated hotspot is then defined as being sourced by a plume (red text in figure); nonplume hotspots are in blue text.

2.1. Plume Advection Models

For each of the four global seismic models, we employ a plume advection model (Steinberger & O'Connell, 1998; Steinberger et al., 2019) to explore how plumes tilt as they upwell through the mantle, which allows us to infer the location of a mantle plume conduit at the core-mantle boundary (CMB) (Text S1 in supporting information). In order to illustrate the effect of choice of seismic model on conduit paths, conduits are shown beneath all hotspots for all four seismic models in Figure 1. We find that conduit paths are broadly similar across the seismic models considered (cf. Boschi et al., 2007), reflective of their similarity in terms of the shear wave velocity anomaly structure at the longest wavelengths (cf. Becker & Boschi, 2002).

2.2. Defining Plume Conduits Beneath Hotspots

A number of approaches have been put forward to identify seismically resolved plume conduits beneath hotspots and their uncertainties (e.g., Boschi et al., 2008; Marignier et al., 2020). Our approach is slightly modified from Boschi et al. (2007): in each seismic model we evaluate the fraction of the mantle's depth (i.e., the plume's "connected conduit length") over which the advected conduits exhibit negative seismic velocity anomalies, and the new method allows for small gaps in the conduit (see Text S1 in supporting information). We average each plume's connected conduit length across the four seismic models, and if the average length is at least 0.6—which corresponds to the conduit spanning 60% of the mantle, and is close to the mean conduit lengths for the hotspots considered—the conduit is categorized as a plume connecting to a hotspot (Figure 2, Table S1). Applying this definition of a plume, 30 of the 58 hotspots examined in this study are associated with seismically imaged mantle plumes.

We use this criterion to define plume-sourced and nonplume hotspots in the remaining figures. Such a global tomographic approach appears useful for identifying presumably wide thermochemical plumes (Boschi et al., 2007; French & Romanowicz, 2015; Marignier et al., 2020), with the caveat that numerous complications exist (e.g., depth-dependent mapping between temperature and velocity anomalies). However, any method based on relatively long-wavelength, global tomography may fail to identify narrower conduits, as expected for purely thermal plumes. Moreover, global tomography does not yet image all the plumes identified in regional studies. For example, the Yellowstone plume is not easily identifiable in any of the four global tomographic models considered; Yellowstone in fact shows the second shortest conduit extent (~0.25) among the 58 hotspots examined (Figure 2). However, the higher resolution afforded by US Array permitted resolution of the Yellowstone plume in a regional seismic model (Nelson & Grand, 2018), and the imaged plume conduit matches dynamic models for the lateral advection of the plume (Steinberger et al, 2019). The Yellowstone case thus suggests that we cannot

Figure 1. Hotspot surface locations (circles colored by inferred plume length) and modeled plume conduits (lines connecting circles to their plume conduit location at the bottom of the mantle) for the four global seismic models considered: (a) S40RTS, (b) SEMUCB-WM1, (c) TX2016, and (d) SMEAN2. Symbol size represents hotspot buoyancy flux in Mg/s (see Table S3). The connected conduit length (i.e., the inferred plume length) is computed based on the extent of slow seismic tomography anomalies along the conduit. Because conduit lengths are normalized to the depth of the mantle, plume conduits that span the whole mantle have values of unity, and hotspots with no resolvable conduit have connected conduit lengths of zero (cf. Boschi et al., 2007; see also Figure 2). Background shows tomographic velocity anomalies at 2,850 km for each seismic model (red-blue scale). The Large Low Shear Wave Velocity Provinces boundaries (based on the −0.75 RMS velocity anomaly) are indicated by magenta lines.

exclude the presence of plumes for the 28 hotspots where global seismic models do not resolve a plume (Figure 2) because future, higher-resolution tomography may yet reveal a deep conduit connection. While connected conduit lengths from global seismic models can underestimate true conduit lengths identified in regional seismic models (e.g., Yellowstone), connected conduits lengths may overestimate the true length of a conduit in other cases: due to convective dynamics a conduit might be disrupted, but global tomography models might smear out significant vertical gaps in a plume (e.g., due to data coverage), with the result being that conduits may not, in fact, be as continuous as they appear in our analysis. However, statistical analysis shows that the match of tomographic anomalies and plume conduits is not simply indicative of broad-scale upwelling, a scenario that would permit a shallow mantle (i.e., nonplume) origin for the hotspots considered here. Instead, correlations between deep conduits and known hotspot locations at the surface are highly significant when considered as a global conduit set (Boschi et al., 2008).

2.3. Defining the LLSVP Boundaries

For each of the seismic models, we define the margins of the two LLSVPs as those shear wave velocity anomalies which are −75% of the root mean square (RMS) velocity anomaly at the CMB (see Text S1 in supporting information). In our earlier work, we found this approach to yield broadly consistent estimates compared to other methods (Jackson et al., 2018b). However, ambiguities as to how LLSVPs are defined can be important, for example when evaluating if plumes are sourced at the edges or interior of LLSVPs (e.g., Austermann et al., 2014; Thorne et al., 2004; Torsvik et al., 2006). We therefore show histograms of inferred plume locations at the base of the mantle (at 2,850 km) as a function of distance from the LLSVP edge (Figure 3). For this, we calculate the shortest distances between the margins of the LLSVPs and downward-projected bases of plume conduits (see Text S1). Using these distances, hotspots are then also classified (for simpler visualization and categorization in some of the figures) as being "far from LLSVP" (i.e., conduit distances are > 500 km outside of the margins of the LLSVPs when averaged across all four seismic models) or LLSVP hotspots (i.e., conduits that are either located within, or not further than 500 km from, the margins of the LLSVPs; cf. Figure 1; Table S1).

Below we examine relationships between hotspot geochemistry and hotspot buoyancy flux (Table S3), advected conduit distances from the margins of the LLSVPs, latitude and longitude of actual conduit base location and seismic velocity anomalies extracted from the advected conduits at 2,850 km. We present relationships using the S40RTS model in Figures 5–8 of the main text, and complementary results for the other seismic models are shown in the Figures S2 through S5.

3. Observations

3.1. Global Relationships Between Hotspots and LLSVPs

To extract some statistical background information from the plume models shown in Figure 1a, Figure 3 displays the global distribution of advected conduit base locations for all 58 hotspots as a function of longitude, latitude (and sin[latitude]), and distance from the LLSVP boundaries. Both vertical conduits, projected downward from the surface hotspot locations (Figures 3a, 3c, and 3e), and advected conduits (Figures 3b, 3d, and 3f), are shown. As expected, the advected hotspot-related plume conduits at the base of the mantle (Figures 3a and 3b) have a bimodal distribution with longitude. This pattern matches the distribution of slow velocity anomalies in tomography in the lowermost mantle (shown with gray lines) that represent the Indo-Atlantic and Pacific LLSVPs (cf. Hager et al., 1985; Richards et al., 1988). The conduit base locations are also shown as a function of latitude (Figures 3c and 3d), indicating a greater number of hotspots in the southern hemisphere, which is again mirrored in deep mantle low seismic velocity anomalies that are also shifted to the southern hemisphere. Compared to vertical conduits, advected conduits reveal a somewhat tighter clustering in the southern hemisphere. Inferred hotspot-related plume base locations are shown as a function of distance from the margins of the LLSVPs in Figures 3e and 3f. There are more hotspots inside the LLSVPs than outside when allowing for plume advection, which contrasts with a random distribution of hotspot conduits (gray line in Figures 3e and 3f). Compared to vertical conduits, which scatter around the margins of the LLSVPs, advected conduits tend to cluster more clearly inside the LLSVPs. Plume conduit base locations are thus associated with LLSVPs, as was suggested based on vertical downward conduit

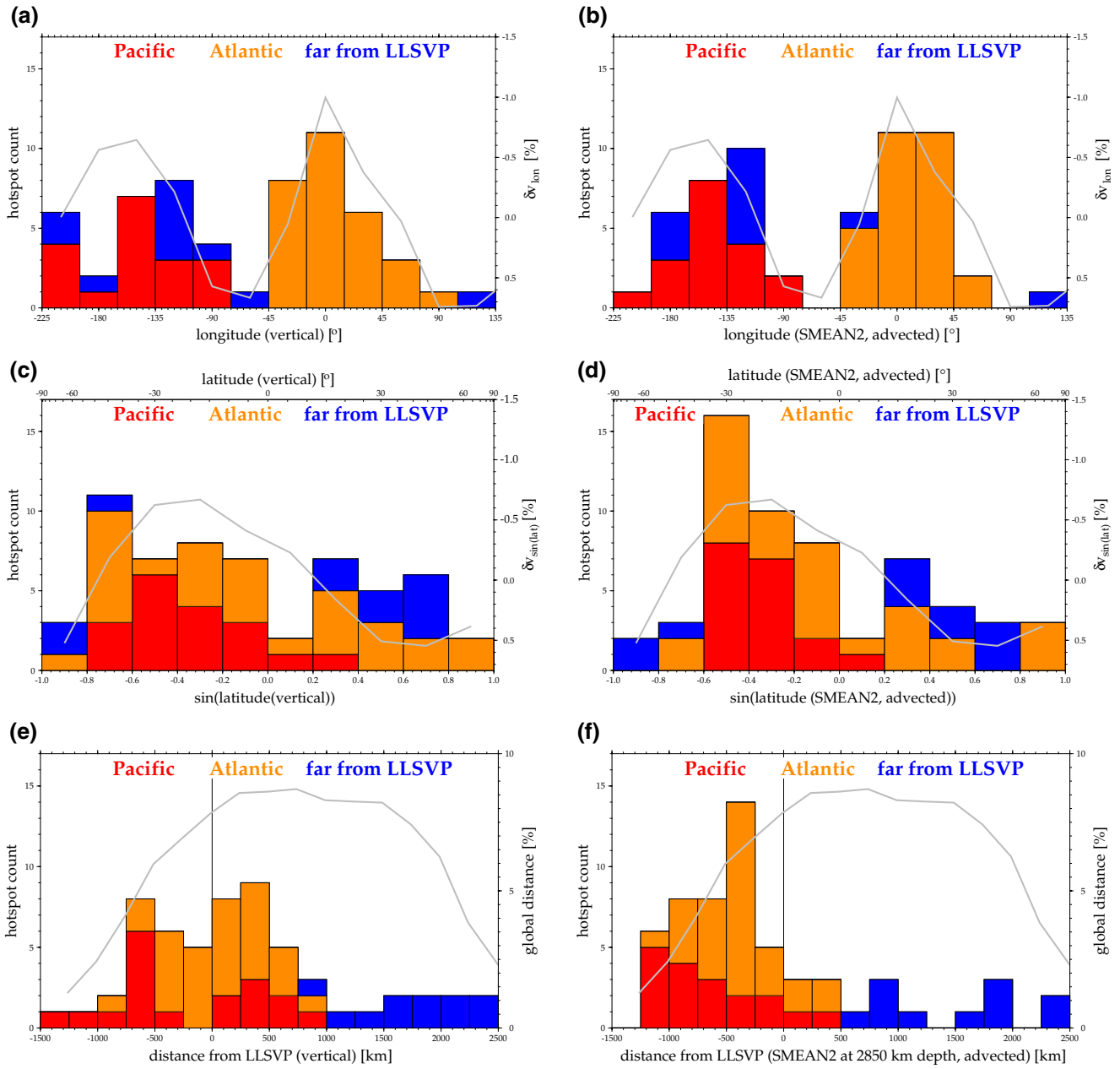

Figure 3. The distribution of conduit locations beneath global hotspots are shown as a function of longitude, sin(latitude) (to account for reduced surface area per degree latitude at higher latitudes), and minimum distance from the margins of the Large Low Shear Wave Velocity Provinces (LLSVPs) at 2,850 km depth (positive distances are outside, negative inside LLSVPs). Results are shown for the SMEAN2 model, but note that the classification into Pacific LLSVP, Indo-Atlantic LLSVP (called "Atlantic" in the figure), and far (>500 km) from LLSVP hotspots is derived from the average of all four tomography models considered (as explained in supporting information Text S1). The histograms count the number of hotspots by bin (Figure S1 is equivalent and uses summed hotspot fluxes). The first column of panels (a, c, and e) assumes *vertical* conduits (projected downward from the surface hotspot locations). The second column (panels b, d, and f) uses conduit bases of *advected* plume conduits at 2,850 km depth. (This distance computation contrasts with the approach taken in Jackson et al. [2018b], where distances between LLSVPs and vertical conduits were projected to the surface.) Results for advected conduits are similar using other seismic models (e.g., S40RTS), and data for generating histograms for advected conduits using other seismic models are available in the Table S1. The gray lines in the top and middle panels show results for shear wave velocity anomalies at 2,850 km for comparison, and thus approximate LLSVP distributions; in the bottom panels, the gray line shows distance distributions for randomly located plumes.

projection (e.g., Richards et al., 1988; Ritsema et al., 2011; Thorne et al., 2004; Torsvik et al., 2006; Williams et al., 1998), and earlier analysis of advected plumes (Boschi et al., 2007). The predominance of plume sources inside the LLSVPs for advected conduits implies that while the temperature gradients at the LLSVP edges might serve to preferentially seed plume instabilities, the conduit base locations might be swept toward the interior subsequently (Steinberger & Torsvik, 2012).

In Figure S1, we also show summed hotspot buoyancy flux distributions using buoyancy estimates provided in Table S3. The results are overall consistent with Figure 3. When considering flux weighted distributions as a function of longitude, the hotspots associated with the Pacific LLSVP form a peak that is more pronounced than that of the Indo-Atlantic LLSVP hotspots, but individual hotspot buoyancy estimates dominate such histograms (e.g., Hawaii, cf. Figures 1a and 4a). Like the distribution of hotspots, the summed hotspot buoyancy fluxes are greater in the southern hemisphere (Figures S1c and S1d), and the clustering of summed hotspot fluxes in the southern hemisphere is more pronounced when using advected plumes. When considering the distances of advected plume conduits from the LLSVPs, most of the plume flux clusters are located within the LLSVPs and have high buoyancy fluxes (approaching 13 Mg/s per bin), while all inferred plume fluxes further than 500 km away from the edges of the LLSVPs are small (<3 Mg/s per bin) (Figure S1f).

3.2. Relationships Between Hotspot Geochemistry and LLSVP Locations

In Figure 4, the lowest $^{143}Nd/^{144}Nd$, highest $^{206}Pb/^{204}Pb$, and highest $^{3}He/^{4}He$ lavas from each hotspot with available geochemical data (see Tables S1 and S2), as well as hotspot buoyancy fluxes (Table S3), are shown in map view. These parameters are also shown in Figure 5 (and Figure S2) as a function of conduit distance from the margins of the LLSVPs.

Hotspots that host only geochemically depleted (high) $^{143}Nd/^{144}Nd$ compositions are found both inside and outside of the LLSVPs. However, the advected conduit base for all hotspots with geochemically enriched (EM) $^{143}Nd/^{144}Nd$ (i.e., $^{143}Nd/^{144}Nd_{sample} \leq 0.512630$; Bouvier et al., 2008) can be traced back to the interiors of, or outside but close to (<500 km) the LLSVPs (Figures 4, 5, and S2). No EM hotspots are found far from the LLSVP boundaries; this substantiates prior work based on vertical plume conduits (Castillo, 1988; Jackson et al., 2018b). However, non-EM hotspots (i.e., geochemically depleted hotspots that lack lavas with $^{143}Nd/^{144}Nd \leq 0.512630$) are likewise found within the LLSVPs, and only about one-third of geochemically characterized oceanic hotspots linked to the LLSVPs exhibit EM signatures. This suggests a heterogeneous distribution of EM and geochemically depleted material in the LLSVPs.

The highest $^{206}Pb/^{204}Pb$ at global hotspots shows no relationship with conduit distance from the LLSVPs (Figures 4, 5, and S2). This observation was made using vertical plume conduits (Jackson et al., 2018b), but is here confirmed with advected conduits and substantiated by incorporating the recent discovery of extremely high $^{206}Pb/^{204}Pb$ in the Bermuda hotspot (Mazza et al., 2019), which is located far from the margins of the nearest (i.e., Indo-Atlantic) LLSVP. Lastly, $^{208}Pb^*/^{206}Pb^*$ ratios associated with the lowest $^{143}Nd/^{144}Nd$ (most EM) lavas from each oceanic hotspot show a clear relationship as a function of conduit distance from the LLSVPs, where high $^{208}Pb^*/^{206}Pb^*$ is associated with the interiors of the LLSVPs. This relationship resembles the strong association between minimum hotspot $^{143}Nd/^{144}Nd$ and the LLSVPs (Figures 5 and S2). In contrast, $^{208}Pb^*/^{206}Pb^*$ ratios associated with the highest $^{206}Pb/^{204}Pb$ (most HIMU) lavas from each oceanic hotspot show no clear relationship with distance from the LLSVPs (Figure 5), resembling the lack of clear relationship between maximum hotspot $^{206}Pb/^{204}Pb$ and distance from the LLSVPs.

With one exception, the highest hotspot buoyancy fluxes, and the highest $^{3}He/^{4}He$ ratios, are linked to advected plume conduits that extend to the interiors of, or outside of but close to both LLSVPs (Figures 4, 5, and S2). However, one moderately high buoyancy flux hotspot (Yellowstone), which also has high $^{3}He/^{4}He$ (19.4 Ra), does not trace back to the LLSVPs. The remaining hotspots located far outside of the LLSVPs have low hotspot buoyancy flux and low $^{3}He/^{4}He$ (Figure 5).

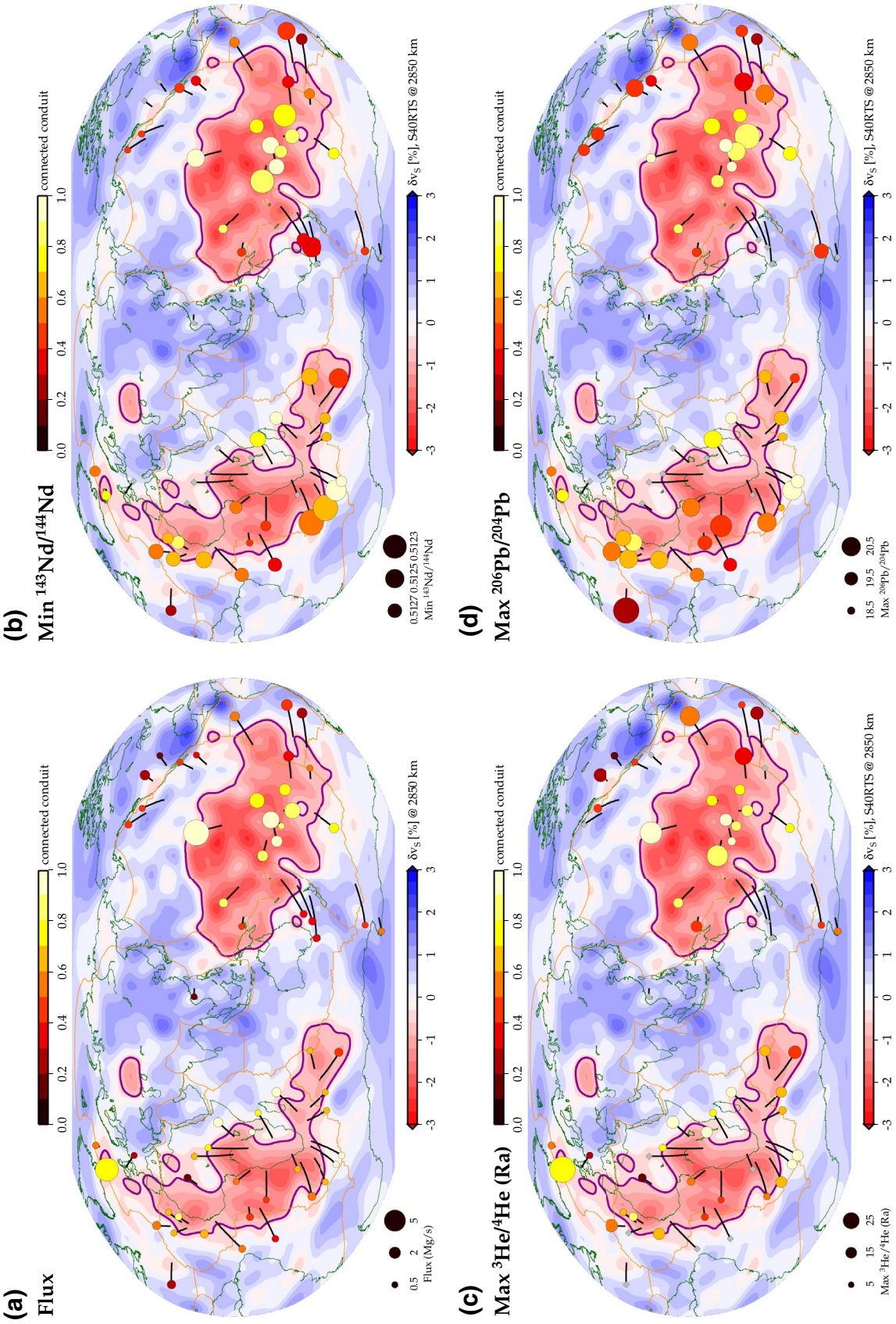
(a)
Flux
(b)
Min $^{143}Nd/^{144}Nd$
(c)
Max $^{3}He/^{4}He$ (Ra)
(d)
Max $^{206}Pb/^{204}Pb$
connected conduit
0.0 0.2 0.4 0.6 0.8 1.0
δv_S [%], S40RTS @ 2850 km
-3 -2 -1 0 1 2 3
Flux (Mg/s)
0.5 2 5
Min $^{143}Nd/^{144}Nd$
0.5127 0.5125 0.5123
Max $^{3}He/^{4}He$ (Ra)
5 15 25
Max $^{206}Pb/^{204}Pb$
18.5 19.5 20.5

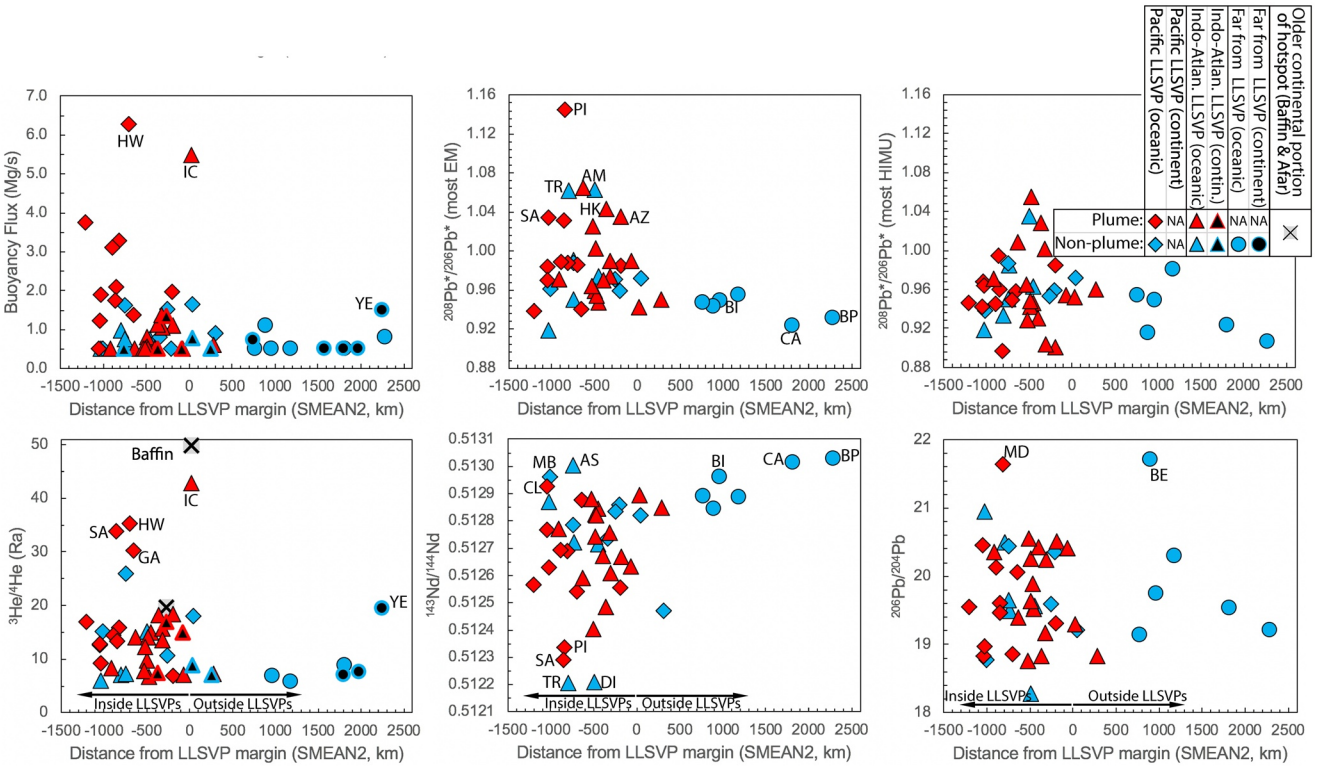

Figure 5. Geochemistry and buoyancy flux of hotspots as a function of conduit distance from the margins of the Large Low Shear Wave Velocity Provinces (LLSVPs). Distances are calculated as minimum distances between the margins of the LLSVPs and downward-projected bases (see Text S1 in supporting information) of advected plume conduits at 2,850 km depth (equivalent plots for SEMUCB-WM1, SMEAN2, and TX2016 are in Figure S2): negative distances are inside of the LLSVPs, positive distances are outside. The values for ^{208}Pb*/^{206}Pb* for the most EM lavas and the ^{208}Pb*/^{206}Pb* for the most HIMU lavas from each hotspot are calculated for the lowest ^{143}Nd/^{144}Nd and highest ^{206}Pb/^{204}Pb samples from each hotspot, respectively. For two hotspots—Iceland and Afar—less radiogenic helium isotope ratios are available on the older continental portions (e.g., Baffin Island) of the hotspots, shown as squares (and complement the data from the younger portions of these hotspots, also included in the figure). Hotspot text labels (e.g., YE = Yellowstone, IC = Iceland) in the figure are defined in Table S1. Maximum hotspot ^{3}He/^{4}He, minimum ^{143}Nd/^{144}Nd, and maximum ^{206}Pb/^{204}Pb are shown to represent expressions of the most primordial component, the strongest EM component, and the strongest HIMU component at each hotspot, respectively (as measured in lavas, see Table S1). Plume related hotspots are red symbols, hotspots without seismically resolved plumes are blue; Pacific LLSVP hotspots are diamonds, Indo-Atlantic LLSVP hotspots are triangles, and far-from-LLSVP hotspots are circles; oceanic hotspots are color filled and continental hotspots are black filled.

3.3. Relationships Between Hotspot Geochemistry and Seismic Shear Wave Velocity Anomalies at the Bottom of the Mantle (2,850 km)

In Figure 6, maximum hotspot ^{3}He/^{4}He, minimum ^{143}Nd/^{144}Nd, and maximum ^{206}Pb/^{204}Pb are shown as a function of the seismic velocity anomaly at 2,850 km in advected plume conduits associated with each hotspot. There is no clear relationship between maximum ^{3}He/^{4}He and shear wave velocity anomalies (δv_s) at the base of related plume conduits. Most high ^{3}He/^{4}He hotspot conduits are associated with low seismic velocity anomalies, but one high ^{3}He/^{4}He hotspot, Yellowstone, is associated with positive δv_s in two of the global seismic tomography models (SMEAN2 and TX2016; Figure S3). In addition, hotspots with low ^{3}He/^{4}He exhibit both positive and negative δv_s.

The relationship between minimum hotspot ^{143}Nd/^{144}Nd and δv_s broadly reflects the relationship between minimum hotspot ^{143}Nd/^{144}Nd and conduit distance from the LLSVPs: EM hotspots are linked to low δv_s, while hotspots lacking EM signatures are associated with both low and high δv_s. However,

Figure 4. Global distribution of hotspot buoyancy flux (a), minimum hotspot ^{143}Nd/^{144}Nd (b), maximum hotspot ^{3}He/^{4}He (c), and maximum hotspot ^{206}Pb/^{204}Pb (d). Shear wave velocity anomalies at 2,850 km in the S40RTS model are shown in the background, and the margins of the Large Low Shear Wave Velocity Provinces are shown as −0.75 RMS velocity contours at 2,850 km (magenta line). Lines connect hotspot locations at the surface (circles) to their plume conduit location at the bottom of the mantle.; the connected conduit length is represented by color at the surface hotspot location; where data are not available, a gray diamond is used. Panel (a) is the same as Figure 1a.

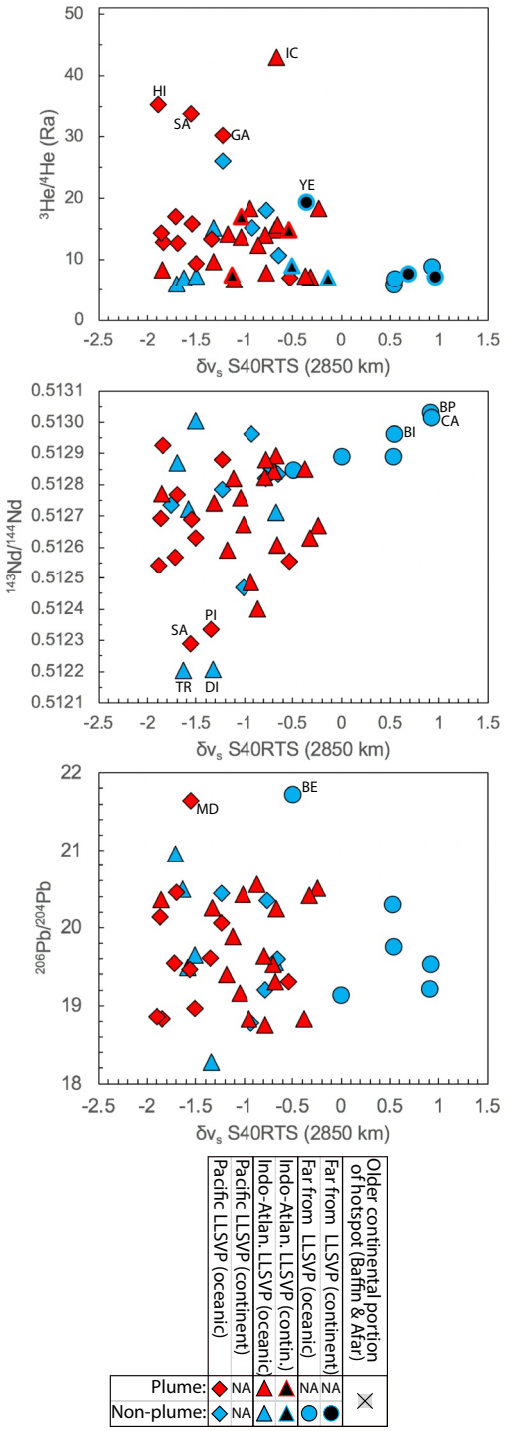

Figure 6. Geochemistry of hotspots as a function of shear wave velocity anomalies at 2,850 km. Velocity anomalies are extracted from advected conduits at 2,850 km using the S40RTS model (equivalent plots for SEMUCB-WM1, SMEAN2, and TX2016 are presented in Figure S3). Maximum hotspot ^{3}He/^{4}He, minimum ^{143}Nd/^{144}Nd, and maximum ^{206}Pb/^{204}Pb are shown to represent expressions of the most primordial component, the strongest EM component, and the strongest HIMU component at each hotspot, respectively (Table S1). Symbols are as described in Figure 5. Hotspot text labels in the figure are defined in Table S1.

we find that the EM Tasmantid hotspot is an exception to this relationship in two global seismic models examined here (SEMUCB-WM1 and SMEAN2; Figure S3). Lastly, we find no correlations between maximum hotspot ^{206}Pb/^{204}Pb and δv_s at 2,850 km.

3.4. Hotspot Geochemistry as a Function of Longitude: Comparing the Geochemistry of the Indo-Atlantic and Pacific LLSVPs

Figure 7 (and Figure S4) shows how the geochemistry of hotspots varies as a function of conduit longitude at the bottom of the mantle. The data appear in two clusters, associated with the Pacific LLSVP and the Indo-Atlantic LLSVP, respectively. The Pacific LLSVP has more hotspots with ^{3}He/^{4}He ≥ 20 Ra, but the Indo-Atlantic LLSVP is host to the highest ^{3}He/^{4}He hotspot, Iceland. While both LLSVPs are linked to hotspots with ^{206}Pb/^{204}Pb ≥ 20, including the second-highest ^{206}Pb/^{204}Pb hotspot (Macdonald), the hotspot with the highest ^{206}Pb/^{204}Pb (Bermuda) is not clearly associated with an LLSVP (see Figure 5, Table S1, Text S1 in supporting information). Hotspots with plume conduits (i.e., connected conduit ≥ 0.6; Figure 2) associated with EM (^{143}Nd/^{144}Nd ≤ 0.512630) signatures are linked to both the Indo-Atlantic LLSVP (five plume-fed EM hotspots, including Amsterdam/St. Paul, Cape Verde, Comores, Kerguelen/Heard, and Meteor/Shona) and the Pacific LLSVP (six plume-fed EM hotspots, including Samoa, Pitcairn, Societies, Hawaii, San Felix, and Rarotonga) (Figure 7). We find that the Pacific LLSVP is linked to more deeply sourced (i.e., plume-fed) EM hotspots than the Indo-Atlantic LLSVP.

3.5. Hotspot Geochemistry as a Function of Latitude

Figure 8 (and Figure S5) show how the geochemistry of hotspots varies as a function of latitude of the plume conduit base. Hotspots that host only geochemically depleted compositions (^{143}Nd/^{144}Nd > 0.512630) are found at all latitudes, but hotspots hosting geochemically enriched compositions (^{143}Nd/^{144}Nd ≤ 0.512630) are found primarily in the southern hemisphere. Across all four seismic models examined here, conduits locations at the CMB show that, north of ~16°N latitude, there are no plumes sourcing EM signatures. Furthermore, EM signatures become more extreme at more southerly latitudes, and all hotspots with the most extreme EM signatures (^{143}Nd/^{144}Nd < 0.5125) are found between 15°S and 43°S. We refer to the band of EM hotspots in the southern hemisphere as the DUPAL domain (Hart, 1984). The DUPAL domain is observed when both plume-fed hotspots and hotspots without resolved plumes are included, or if only plume-fed hotspots are examined (Figure S5). While the LLSVPs are shifted toward the southern hemisphere—showing peaks in their distribution at ~20°S (gray line in Figure 3c)—the DUPAL domain is shifted even further south (i.e., from 15°S to 43°S) and toward the southern regions of the LLSVPs.

Maximum hotspot ^{3}He/^{4}He and minimum ^{143}Nd/^{144}Nd show possibly complementary trends with latitude: the most extreme EM signatures are concentrated toward the southernmost latitudes while the highest ^{3}He/^{4}He is present in high-northern latitudes (farthest from the EM DUPAL domain). The upper envelope for maximum ^{3}He/^{4}He with latitude is anchored by the Iceland hotspot, but possible complementary DUPAL (southern hemisphere) and high ^{3}He/^{4}He (northern hemisphere) domains are nonetheless notable (Figures 8 and S5). Lastly, the two hotspots with the highest ^{206}Pb/^{204}Pb—Macdonald and Bermuda—are located in the tropical latitudes (Figure S5).

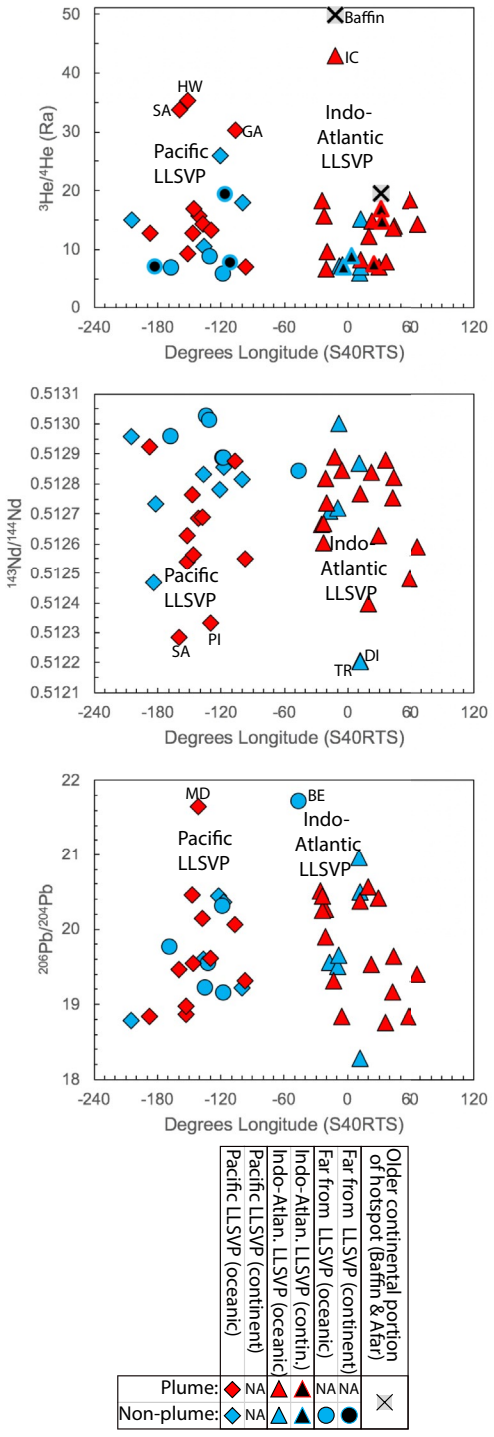

Figure 7. Geochemistry of hotspots as a function of longitude of the plume conduit at 2,850 km depth using the S40RTS global seismic model (equivalent plots for SEMUCB-WM1, SMEAN2, and TX2016 in Figure S4). Maximum hotspot ^{3}He/^{4}He, minimum ^{143}Nd/^{144}Nd, and maximum ^{206}Pb/^{204}Pb are shown to represent expressions of the most primordial component, the strongest EM component, and the strongest HIMU component at each hotspot, respectively (Table S1). The highest ^{3}He/^{4}He portion of the proto-Iceland plume (i.e., Baffin Island), and the Afar hotspot, are shown for reference. Symbols are as described in Figure 5. Hotspot text labels in the figure are defined in Table S1.

3.6. Relationships Between Hotspot Geochemistry and Buoyancy Flux

Figure 9 shows the maximum ^{3}He/^{4}He, minimum ^{143}Nd/^{144}Nd, and the maximum ^{206}Pb/^{204}Pb of hotspots as a function of hotspot buoyancy flux. Maximum ^{3}He/^{4}He at hotspots shows a positive correlation with hotspot buoyancy flux, where the Spearman's rank correlation coefficient for all hotspots is $r_s = 0.57 \pm 0.11$ (with 1σ error calculated using bootstrap as described in Jackson et al., 2017). This observation is consistent with prior findings (Graham, 2002; Jackson et al., 2017; Jellinek & Manga, 2004; Putirka, 2008). However, minimum hotspot ^{143}Nd/^{144}Nd and maximum ^{206}Pb/^{204}Pb at hotspots show no apparent relationship with hotspot buoyancy flux.

4. Discussion

4.1. Enriched Mantle Domains Geographically Linked to Both LLSVPs

The conduits of all EM hotspots can be traced back to the interiors of, or close to (<500 km) the LLSVPs (Figure 5). Furthermore, both LLSVPs source EM hotspots. If we limit our analysis to only the hotspots linked to seismically defined plumes (Figure 2), we still find that both LLSVPs are associated with EM hotspots. This suggests a strong association between subducted continental crust material (White & Hofmann, 1982) and the LLSVPs (Castillo, 1988; Jackson et al., 2018b).

We started our analysis prior to the publication of Doucet et al. (2020), but have to note how our observations contrast with their findings. Doucet et al. (2020) argue that only the Indo-Atlantic LLSVP sources EM hotspots, and that the Pacific LLSVP is devoid of EM domains. The authors suggest that, over the supercontinent cycles, continental crust material has been delivered only to the Indo-Atlantic, and not to the Pacific LLSVP. It is unclear to us which deterministic geodynamic mechanism would favor crust delivery to one LLSVP, but not the other, over multiple supercontinent cycles (i.e., Pangea, Rodinia, Columbia/Nuna, and Kenorland).

The difference in conclusions relates, in part, to data selection. Doucet et al. (2020) suggest that identification of a seismically resolved plume extending into the deep mantle is insufficient to evaluate whether the hotspot is fed by a plume of "deep origin". Instead, they argue that four additional criteria must be met before a seismically resolved plume can be considered deeply sourced (cf. Courtillot et al., 2003): the hotspot must also be associated with a flood basalt, the hotspot must be linked to a long-lived hotspot track, the hotspot must have high ^{3}He/^{4}He ratios (>10 Ra), and a hotspot must be located far from a subduction zone. As a consequence, Doucet et al. (2020) exclude a number of hotspots we identify as deeply sourced hotspots (due to association with seismically resolved conduits; Figure 2) that emerge from the Pacific (e.g., Pitcairn, Societies, Marquesas, Macdonald, and Caroline) and Indo-Atlantic (e.g., Cameroon, Canary, Cape Verde, and Comores) LLSVPs. Critically, many of the hotspots excluded by Doucet et al. (2020) are actually EM hotspots linked to the Pacific LLSVP via deep plume conduits (e.g., Pitcairn, Samoa, Societies, etc.), thereby weakening the hypothesis that the Pacific LLSVP does not host EM material. Making the seismic definition of a plume secondary to surface features (ancient flood basalts, long-lived hotspot tracks, proximity to trenches), or hotspot lava geochemistry (high ^{3}He/^{4}He) may lead to an inaccurate geochemical representation of the deep mantle sampled by plume-fed hotspots. When defining plumes using seismic tomography and geodynamics as we do here, subducted continental crust material sampled by hotspots appears linked to both LLSVPs, not just one.

In contrast to the suggestion that subducted continental crust is geographically restricted to both LLSVPs (Castillo, 1988; Jackson et al., 2018b), Williams et al. (2019)

argue that recycled crust exhibits no significant relationship with either LLSVP. Williams et al. (2019) used maximum $^{208}Pb^*/^{206}Pb^*$ at hotspots as a proxy for recycled crust, and suggested that maximum $^{208}Pb^*/^{206}Pb^*$ (and therefore recycled crust) exhibits no significant relationship with the low-velocity regions of the deep mantle (Williams et al., 2019). This contrasts with our result of an association between EM (low $^{143}Nd/^{144}Nd$)—sourced by recycled continental crust—and the LLSVPs. This discrepancy may be due to the fact that $^{208}Pb^*/^{206}Pb^*$ is an imperfect proxy for $^{143}Nd/^{144}Nd$: a plot of $^{143}Nd/^{144}Nd$ versus $^{208}Pb^*/^{206}Pb^*$ for global OIB data only hints at a negative correlation (see Figure 15 of Hofmann, 2014). Nonetheless, we find that if the $^{208}Pb^*/^{206}Pb^*$ value associated with the lowest $^{143}Nd/^{144}Nd$ lava from each oceanic hotspot (Table S1) is plotted as a function of conduit distance from LLSVPs, then high $^{208}Pb^*/^{206}Pb^*$ is clearly associated with the LLSVPs (see Figure 5), consistent with the association of low $^{143}Nd/^{144}Nd$ with the LLSVPs. In contrast, when the $^{208}Pb^*/^{206}Pb^*$ value associated with the highest $^{206}Pb/^{204}Pb$ at each hotspot (Table S1) is plotted against conduit distance from the LLSVPs, no clear relationship emerges (Figure 5). This is reminiscent of the lack of relationship between maximum hotspot $^{206}Pb/^{204}Pb$ and conduit distance from the LLSVPs (Figure 5). Therefore, our results suggest that, in order to use $^{208}Pb^*/^{206}Pb^*$ as a tool for tracing the geographic relationships between recycled reservoirs and the LLSVPs, it is important to first distinguish between EM (i.e., minimum hotspot $^{143}Nd/^{144}Nd$, which shows a clear geographic relationship with the LLSVPs) and HIMU (i.e., maximum hotspot $^{206}Pb/^{204}Pb$, which shows no geographic relationship with the LLSVPs) components at hotspots. We thus do not find that $^{208}Pb^*/^{206}Pb^*$ excludes a relationship between subducted continental crust and the LLSVPs. The clear relationship between minimum hotspot $^{143}Nd/^{144}Nd$ and conduit distance from the LLSVPs (Figure 5) provides strong evidence for subducted continental crust being geographically accumulated in the two LLSVPs.

Before accepting a model where EM material is geographically predisposed to the LLSVPs, it is important to consider, and possibly refute, a model where the distribution of EM material is similar inside and outside of the LLSVPs, but is not entrained by plumes outside of the LLSVPs. For example, if EM domains are anomalously dense, they would be entrained only by the most buoyant plumes, which tend to be associated with the LLSVPs (Figure 5). In this scenario, the less buoyant plumes outside of the LLSVPs may be unable to entrain dense EM material located outside of the LLSVPs. Such a model would predict a negative correlation between minimum $^{143}Nd/^{144}Nd$ and buoyancy flux at hotspots (Figure 9), but no such correlation is observed. This observation argues against a model where dense EM domains lie outside the LLSVPs, but are too dense to be entrained by the relatively weak non-LLSVP plumes (Jackson et al., 2018b).

It is also unlikely that EM domains exist in the same abundance inside and outside of the LLSVPs but, by chance, hypothetical EM domains outside of the LLSVPs are not sampled by plumes. Of the 46 oceanic hotspots characterized for $^{143}Nd/^{144}Nd$, six are consistently positioned far outside of the margins of the LLSVPs, and they are geochemically depleted with $^{143}Nd/^{144}Nd \geq 0.512844$ (i.e., 0.512844 is the lowest $^{143}Nd/^{144}Nd$ value reported among the six hotspots located far from the LLSVPs, and was measured in a Bermuda hotspot lava; see Table S1). In contrast, only 9 of the 40 geochemically characterized oceanic hotspots linked to the LLSVPs are similarly depleted (i.e., all lavas measured from these nine LLSVP-linked hotspots have $^{143}Nd/^{144}Nd \geq 0.512844$), while the other 31 LLSVP hotspots host a less geochemically depleted component (i.e., at least one lava from each of these 31 hotspots has $^{143}Nd/^{144}Nd < 0.512844$). If we assume that the mantle outside the LLSVPs has the same distribution of geochemically depleted and geochemically enriched materials as the mantle within the LLSVPs, then the probability that the more geochemically enriched component is not sampled by the six hotspots outside of the LLSVPs is $p = 0.013\%$ (i.e., $[9/40]^6$). It is therefore unlikely that material with less geochemically depleted $^{143}Nd/^{144}Nd$ (<0.512844) is just as common outside of the LLSVPs as it is inside. Geochemical and geophysical constraints thus support a strong geographic relationship between EM domains and both of the LLSVPs (cf. Castillo, 1988; Jackson et al., 2018b).

While low $^{143}Nd/^{144}Nd$ EM domains are uniquely associated with the LLSVPs, the EM material is not evenly distributed throughout the LLSVPs. Instead, the most geochemically extreme EM material ($^{143}Nd/^{144}Nd < 0.5125$) is sampled primarily by plume conduits that extend into the southern portions (from 43°S to 15°S) of both LLSVPs, and only geochemically depleted ($^{143}Nd/^{144}Nd > 0.512630$) hotspots are found north of 16° N. While well established (Castillo, 1988; Hart, 1984; Jackson et al., 2018b), the concentration of EM domains in the southern hemisphere is important as it contrasts with results from Doucet

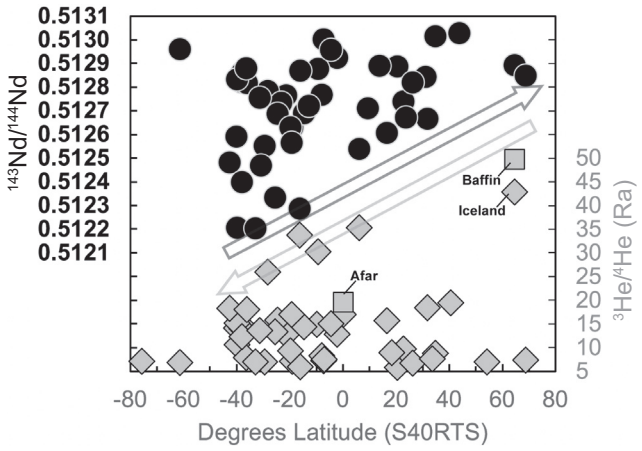

Figure 8. Geochemistry of hotspots as a function of latitude of the plume conduit at 2,850 km depth using the S40RTS global seismic model. Equivalent plots showing plume and Large Low Shear Wave Velocity Province classification for all relevant seismic models—S40RTS, SEMUCB-WM1, SMEAN2, and TX2016—are presented in Figure S5. Gray symbols represent $^{3}He/^{4}He$ data, and black symbols represent $^{143}Nd/^{144}Nd$ data. Maximum hotspot $^{3}He/^{4}He$ and minimum $^{143}Nd/^{144}Nd$ are shown to represent expressions of the most primordial component and the strongest EM component, respectively (Table S1). For two hotspots—Iceland and Afar—higher $^{3}He/^{4}He$ are available on the older continental portions (e.g., Baffin Island) of the hotspots (and complement the high $^{3}He/^{4}He$ data from the younger portions of these hotspots, also included in the figure).

et al. (2020), who concluded that plumes of deep origin in the southern hemisphere are no more likely to sample EM domains than deep-seated plumes in the northern hemisphere. Again, our difference in conclusion appears to be due to data selection.

It is still not known what mechanism is responsible for concentrating EM material in the southern hemisphere, as subduction injection of continental material over geologic time should generate a random geographic distribution of EM material in the mantle (Hart, 1984; Jackson et al., 2018b), not the observed geographic bias of EM material in the southern hemisphere. However, given that EM is generated by continental crust recycling, the concentration of a deep, isolated EM domain in the southern hemisphere would appear to require preferential subduction in the southern hemisphere (Dupré & Allègre, 1983; Hart, 1984; White, 2015), possibly around the perimeter of a supercontinent during a period of anomalously high-subduction flux (Jackson et al., 2007b). While this mechanism could contribute to the hemispheric pattern of geochemical enrichment that is characteristic of the DUPAL, such a scenario requires high viscosity in the lower mantle, otherwise subsequent subduction could push subducted continental materials into the northern hemisphere. Conversely, in this scenario, material subducted in the northern hemisphere, or near the equator, could have been pushed into the southern hemisphere if plates move predominantly northward and get subducted in the north, and induce a southward return flow in the deep mantle. This effect of a degree-1 convection regime (e.g., Zhong et al., 2007) will be pronounced if there is a layer of sufficiently low viscosity at the base of the mantle: advection velocities for subducted materials in the deepest mantle may be on the order of cm/year if viscosities are similar to the asthenosphere (e.g., Steinberger & Calderwood, 2006) (and not higher, as suggested elsewhere; e.g., Rudolph et al., 2015).

Other factors may also conspire to make it difficult to map paleo subduction locations onto the DUPAL. For example, convection at present is, of course, dominated by degree-2 (Steinberger & Calderwood, 2006) and expected to be only intermittently in degree-1, and not necessarily to have North-South alignment (e.g., Zhong et al., 2007) like the DUPAL. In addition, subducting slabs may require up to ~200 Ma to descend to the bottom of the mantle (Domeier et al., 2016; van der Meer et al., 2010), and it may take another few tens to ~100 Ma for slab materials to rise to the surface in upwelling plumes. (Such estimates for plume transit times across the mantle—obtained from the plume fluxes as listed (Table S3) and a diameter of 100–200 km for the central part of the conduit through which most of the flux occurs—are similar to estimates of plume head rise time (Steinberger et al., 2019; Torsvik et al., in press), and should not be much longer in duration because the conduit would then disconnect from the plume head.) Therefore, even in the limiting case where subducted material is returned to the surface immediately after reaching the bottom of the mantle, some delay (up to ~300 Ma) is expected between subduction and the appearance of recycled crustal materials in hotspot lavas, and an even longer delay is expected if the subducted materials remain at the bottom of the mantle for any length of time (i.e., a long residence in the mantle for at least some recycled crust is suggested by geochemical signals in OIB; Cabral et al., 2013; Castillo et al., 2018; Chauvel et al., 1992; Eisele et al., 2002; Galer et al., 1985; Hanyu et al., 2011; Hart, 1984; Hauri & Hart, 1993; Hofmann, 2014; Hofmann & White, 1982; Stracke, 2012). Additional complexity arises from uncertainty in the paleo-arrangement of subduction zones prior to the Neoproterozoic, and subducted sediment fluxes are even more poorly constrained further back in time. Therefore, poor paleographic and paleo-subduction sediment flux records, delay between crustal subduction and upwelling in plumes, and possible advection of subducted crust in the deep mantle in response to subduction and plate motion at the surface, make it difficult to link the geographic distribution of the DUPAL anomaly to paleo subduction zones.

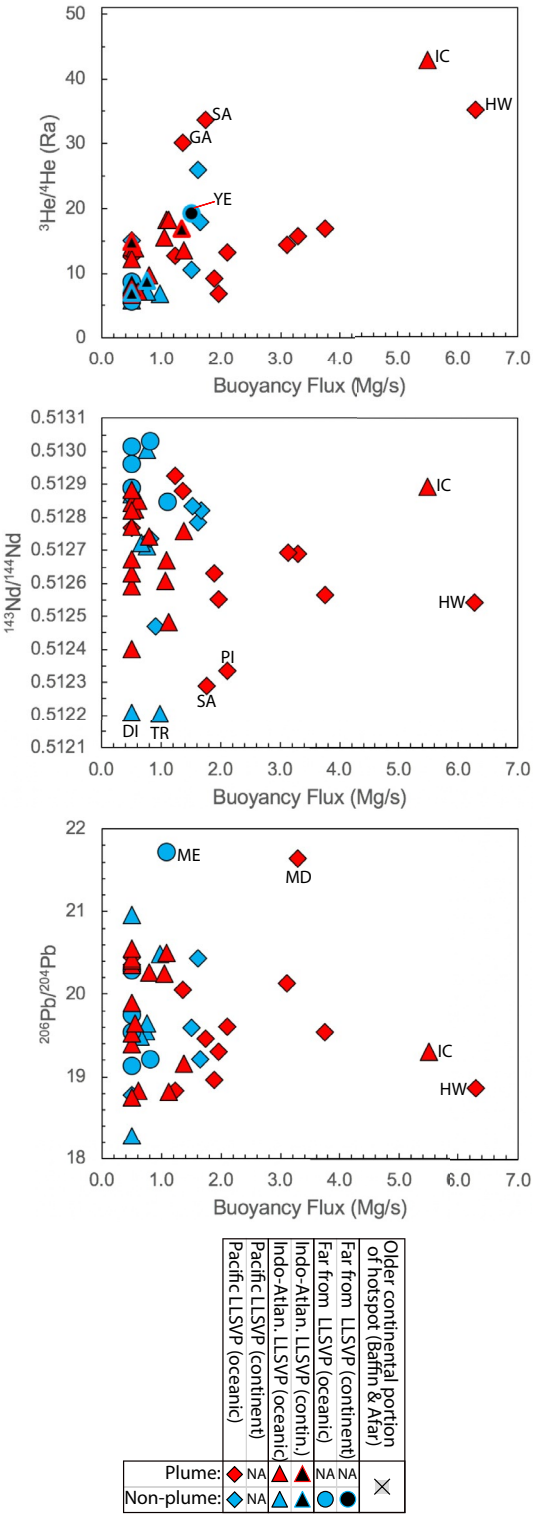

Figure 9. Hotspot geochemistry as a function of hotspot buoyancy flux. Buoyancy fluxes are compiled in Table S3. Maximum hotspot ^{3}He/^{4}He shows a positive relationship with hotspot buoyancy flux, but minimum ^{143}Nd/^{144}Nd and maximum ^{206}Pb/^{204}Pb at global hotspots show no relationship with buoyancy flux. Hotspot text labels (e.g., YE = Yellowstone, IC = Iceland) in the figure are defined in Table S1. Symbols are as described in Figure 5.

4.2. Why Are EM Hotspots Confined to the LLSVPs, but HIMU Hotspots Are Everywhere?

In contrast to EM, HIMU shows no association with the LLSVPs (Figure 5). If EM and HIMU are generated by subduction of continental and oceanic crust, respectively (Hofmann & White, 1982; White & Hofmann, 1982), and if continental and oceanic crust are part of the same subduction package and enter the mantle together in downgoing slabs, a key question is why EM (restricted to the LLSVPs) and HIMU (not restricted to the LLSVPs) domains are geographically decoupled.

One possibility is that, unlike EM domains, which are composed of recycled continental crust (Jackson et al., 2007a; White & Hofmann, 1982), HIMU domains are not composed of material linked to downgoing slabs. If this is the case, there would be no reason for EM and HIMU to be spatially coupled in the mantle. For example, one recent model suggests that HIMU is ancient, carbonatite metasomatized subcontinental lithospheric mantle (SCLM; Weiss et al., 2016), and another model argues for a carbonatite origin for HIMU at the CMB (Collerson et al., 2010). Neither model for HIMU is explicitly linked to downgoing slabs. However, a recycled oceanic crust protolith is still the most plausible model for generation of HIMU. For example, elevated Ti concentrations in HIMU lavas are not explained by the two models above (Collerson et al., 2010; Weiss et al., 2016), but are explained by a mafic contribution (Davis et al., 2011; Prytulak & Elliott, 2007). In addition, sulfur isotopic compositions in HIMU lavas are linked to Archean recycled hydrothermally altered oceanic crust (Cabral et al., 2013). Third, radiogenic ^{187}Os/^{188}Os signatures in HIMU lavas (e.g., Hanyu et al., 2011; Hauri & Hart, 1993) are not present in SCLM (except at a single Siberian locality where the ^{187}Os/^{188}Os is a syn- or posteruptive feature and therefore not interpreted to reflect the SCLM composition; Ionov et al., 2015), but are characteristic of ancient recycled oceanic crust, signaling the importance of a mafic contribution to HIMU lavas.

However, one issue with a recycled oceanic crust origin for HIMU is that HIMU lavas are relatively uncommon among OIB globally, which contrasts with the relatively large volumes of oceanic crust that are inferred to have accumulated in the deep mantle over geologic time. One explanation for the relative rarity of HIMU OIB is that only ancient subducted oceanic crust has had sufficient time to generate extreme HIMU compositions (i.e., Cabral et al., 2013), while younger subducted oceanic crust—which may be abundant in the mantle and in the sources of OIB (e.g., Chauvel et al., 1992; Eisele et al., 2002; Stracke, 2012)—has not had sufficient time to evolve extreme high ^{206}Pb/^{204}Pb ratios. In short, there is no reason to expect all oceanic crust, especially young oceanic crust, to be HIMU in composition. In addition, oceanic crust subducted to the CMB is likely to be denser than ambient mantle at these depths, making subducted oceanic crust more difficult to entrain in upwelling plumes, which may also help explain the rarity of HIMU in OIB in spite of the inferred abundance of subducted oceanic crust in the deep mantle. This model can also help explain the lack of correlation between ^{206}Pb/^{204}Pb and hotspot buoyancy flux (Figure 9) because, if subducted oceanic crust has heterogeneous ^{206}Pb/^{204}Pb as a function of its age, then high buoyancy flux plumes will entrain oceanic crust with both high and low ^{206}Pb/^{204}Pb.

Assuming that EM and HIMU arise from subduction of continental and oceanic crust, respectively, we propose a conceptual model below for the spatial decoupling of EM and HIMU domains in the mantle. The position of global subduction zones anticorrelates geographically with the locations of the LLSVPs. This is expected for whole mantle convection because of the near symmetric distribution of slow and fast velocity anomalies (e.g., Yanagisawa & Hamano, 1999), and because slabs are expected to push any compositional component of LLSVPs or any deep global com-

positional layer around at the base of the mantle (e.g., McNamara & Zhong, 2005; Zhang et al., 2010). A pattern of mantle convection characterized by subduction downwelling around the LLSVPs, and upwelling over the LLSVPs (supported by higher plume flux over the LLSVPs; Figures 3 and 5), will tend to draw subducted material into the LLSVPs as material subducted outside of the LLSVPs is pushed toward the LLSVPs by downgoing slabs (Boschi et al., 2008; Bower et al., 2013; Tan et al., 2002; Zhang et al., 2010; Zhong et al., 2007). As a result, the LLSVPs are expected to have accumulated substantial quantities of subducted continental and oceanic crust over geologic time.

In contrast, there is less oceanic crust and continental crust outside the LLSVPs (because subducted crust is swept into the LLSVPs), and far less continental crust than oceanic crust both outside and inside of the LLSVPs (because less continental crust is subducted into the mantle relative to oceanic crust). The distribution of continental and oceanic crust inside and outside of the LLSVPs will impact the degree to which EM and HIMU domains, respectively, are entrained in plumes. The two primary limitations on entrainment of subducted crust by plumes are the entrainment capacity of a plume (which limits entrainment of materials that are abundant in the plume feeding zone, like oceanic crust inside and outside of the LLSVPs), and the amount of material available to be entrained (which is the key limitation for entrainment of materials that are relatively scarce in the plume feeding zone, such as continental crust outside LLSVPs).

In this model, the abundance of oceanic crust (and thus HIMU) in regions both inside and outside of the LLSVPs is sufficiently high that entrainment is limited by the entrainment capacity of the plume (i.e., the amount of chemically denser material the plume is able to entrain and still be able to rise to the surface), explaining the presence of HIMU signatures in both LLSVP and non-LLSVP hotspots. Therefore, no correlation between oceanic crust and LLSVPs is expected to be observed in OIB. In contrast, it is possible that entrainment of subducted continental material, which is less abundant in the deep mantle than oceanic crust, is primarily limited by the amount available in the plume feeding zone. There should therefore be more continental crust entrained in plumes (and sampled by plume-sourced OIB lavas) that stem from the LLSVPs, where there is more continental crust available, and less continental crust entrained in plumes located far from the LLSVPs, where there is less continental crust available. However, not all of the LLSVP plumes host an EM signature—only about 1/3 of geochemically characterized LLSVP hotspots exhibit EM signatures—and this can be explained if the subducted continental crust material is not necessarily everywhere in the LLSVPs. This is supported by the observation that EM signatures are found almost exclusively in the southern (DUPAL) regions of the LLSVPs.

While this simple conceptual model helps to explain why EM is found only in LLSVP-linked hotspots and HIMU is found in hotspots everywhere, it does not explain the observation that the Pacific LLSVP is primarily linked to EM2-flavored hotspots (but does host at least one EM1 hotspot, Pitcairn, and a possible EM1 signature at Hawaii; Weis et al. [2011]) while the Indo-Atlantic LLSVP is dominated by EM1 hotspots (White, 2015). Understanding the origin of this geochemical difference will be important for constraining possibly dissimilar histories for the LLSVPs.

4.3. A Link Between Primordial High $^3He/^4He$ and the LLSVPs?

While EM signatures resulting from subducted continental crust materials are geographically linked to the LLSVPs, an important question is whether the high $^3He/^4He$ domain is also geographically restricted to the LLSVPs, as suggested previously (Williams et al., 2019). Given that the Yellowstone observation does not support the high $^3He/^4He$ domain being geographically restricted to the LLSVPs, we reexamine the relationship between primordial helium and the LLSVPs below.

Due to assimilation of ancient ^4He-rich continental crust during magmatic ascent (Chiodini et al., 2012; Lowenstern et al., 2014), the elevated $^3He/^4He$ of the Yellowstone mantle plume is likely to be even higher than the $^3He/^4He$ ratios of 19.4 Ra measured in lavas (Graham et al., 2009), and there are hints of this in the literature: for example, a higher $^3He/^4He$ value of 25 ± 4.4 Ra (1σ) (Abedini et al., 2006) was measured in a Yellowstone lava, but this value is associated with larger uncertainties. Similarly, a value of 24.2 ± 2.8 Ra was reported by crushing olivine separates associated with glacial moraines near Yellowstone (Licciardi et al., 2001), but higher $^3He/^4He$ (92.6 Ra) was obtained by fusion of the crushed olivines, and more work is

needed to exclude a cosmogenic ^{3}He component in the crushing experiment. Nonetheless, it is clear that a primordial component exists in the Yellowstone plume (e.g., Broadley et al., 2020; Labidi et al., 2020), and a deep plume source for Yellowstone (Nelson & Grand, 2018; Steinberger et al., 2019) is evidence that elevated ^{3}He/^{4}He exists outside of the LLSVPs in the deep mantle.

Yellowstone may not be the only example of a non-LLSVP hotspot hosting elevated ^{3}He/^{4}He. Basu et al. (1996) reported ^{3}He/^{4}He of up to 12.7 Ra in ~250 Ma Siberia flood basalts, and absolute plate motion models do not link this flood basalt province geographically with the current location of the LLSVPs (Torsvik et al., 2006; Torsvik et al., 2008). Thus, evidence from the high ^{3}He/^{4}He Yellowstone hotspot, and possibly the Siberian flood basalts, lead us to conclude that, while most high ^{3}He/^{4}He hotspots are linked to the LLSVPs, there appear to be elevated ^{3}He/^{4}He domains located in the mantle outside of the LLSVPs.

Furthermore, results from some seismic models suggest that the northernmost portion of the Indo-Atlantic LLSVP, which sources the highest ^{3}He/^{4}He hotspot (Iceland), is not contiguous with the main body of the Indo-Atlantic LLSVP (Figure 1). This is one example of LLSVPs perhaps consisting of an amalgamation of patches of distinct material, such as at the base of a "plume forest" (e.g., Davaille, 1999; Davaille & Romanowicz, 2020; Schubert et al., 2004), rather than being monolithic, coherent reservoirs sourcing plumes. Together, these observations make it important to consider the morphology, plume forest versus monolithic structure, of the LLSVPs when considering models for geochemical reservoirs that are geographically restricted to the LLSVPs.

The relationship between maximum ^{3}He/^{4}He and hotspot buoyancy flux does provide important clues regarding the nature and distribution of the high ^{3}He/^{4}He domain. Unlike minimum hotspot ^{143}Nd/^{144}Nd and maximum ^{206}Pb/^{204}Pb, the maximum ^{3}He/^{4}He at global hotspots correlates with hotspot buoyancy flux (Figure 9). This observation is consistent with a model where the high ^{3}He/^{4}He domain is deep and dense (Jellinek & Manga, 2004), and therefore entrained only by the hottest and most buoyant plumes (Jackson et al., 2017) (Figure 9). This model may help to explain why Yellowstone is the only modern high ^{3}He/^{4}He hotspot located far outside of the LLSVPs: while non-LLSVP hotspots tend to have low hotspot buoyancy fluxes compared to LLSVP-linked hotspots (Figure 5), the Yellowstone hotspot is the only modern hotspot with a relatively high-buoyancy flux located outside of the LLSVPs, and therefore the only non-LLSVP hotspot with sufficient buoyancy to entrain a dense high ^{3}He/^{4}He layer that is not geographically restricted to the LLSVPs. Thus, the Yellowstone example (and possibly the Siberian flood basalts, which presumably would have been fed by a high buoyancy plume, given the nature of the large volume of this flood basalt province) suggests that it is not the geographic position of a hotspot with respect to the LLSVPs that determines whether a hotspot has high ^{3}He/^{4}He (Williams et al., 2019), but it is instead an intrinsic property of a plume—the plume's temperature and buoyancy flux, and therefore entrainment potential—that determines whether a potentially widespread (both inside and outside of the LLSVPs) and dense high ^{3}He/^{4}He material is entrained. The observation that high ^{3}He/^{4}He is rarely entrained outside of the LLSVPs is not necessarily evidence for a paucity of high ^{3}He/^{4}He material outside of the LLSVPs, but can also be attributed to a paucity of high buoyancy plumes outside of the LLSVPs capable of entraining a dense high ^{3}He/^{4}He domain that could be broadly distributed in the deep mantle.

If the high ^{3}He/^{4}He reservoir is dense and broadly distributed at the CMB, both inside and outside of the LLSVPs, an important question is why, unlike subducted crust, high ^{3}He/^{4}He material is not pushed by downgoing slabs and concentrated within the LLSVPs. This needs to be explored further with dynamic models. However, one possible alternative to a widespread and dense high ^{3}He/^{4}He mantle domain, which is not guided into the LLSVPs by downgoing slabs, would be a core origin for primordial ^{3}He/^{4}He (Bouhifd et al., 2013, 2020; Macpherson et al., 1998; Porcelli & Halliday, 2001; Starkey et al., 2009) that manifests in localized pockets of dense silicate melt at the CMB. If core-derived helium is partitioned into silicate melt pockets at the CMB in much the same way that tungsten is argued to partition from the core into deep mantle silicate melts (Mundl-Petermeier et al., 2020), then anomalous ^{182}W and high ^{3}He/^{4}He may reside in silicate melt pockets at the CMB. This model would help explain the observation that anomalous ^{182}W in OIB, suggested to be a core signature, is found only in high ^{3}He/^{4}He lavas (Mundl et al., 2017). Ultra-low velocity zones (ULVZs) may reflect partial melts at the CMB (Williams & Garnero, 1996), possibly at the base of upwelling plumes (e.g., Cottaar & Romanowicz, 2012; Kim et al., 2020; Thorne et al., 2013; Yuan & Romanowicz, 2017). If deep silicate melts just above the CMB are dense and sink to accumulate as ULVZs

(Andrault et al., 2017), they would satisfy the requirement that the high $^{3}He/^{4}He$ reservoir is dense and entrained by only the most buoyant plumes (Jackson et al., 2017). Yu and Garnero (2018) showed that, while ULVZs tend to be concentrated in the LLSVPs, some ULVZs exist outside of the LLSVPs, which is consistent with the observation that most high $^{3}He/^{4}He$ hotspots are located inside the LLSVPs, and some (e.g., Yellowstone, Siberian flood basalts) exist outside. If ULVZs have high $^{3}He/^{4}He$ from the core and are temporally short-lived features—which appear (as silicates melts above the CMB) as plumes form and disappear (solidify) as plumes die—then the fleeting existence of ULVZs would make it difficult for them to be effectively guided into the LLSVPs by downgoing slabs over geologic time. This model may help explain why some high $^{3}He/^{4}He$ sources to plumes are geographically linked to the LLSVPs, but others (Yellowstone, Siberian flood basalts) are not.

4.4. Preserving the Highest $^{3}He/^{4}He$ Outside of the DUPAL Domain

The complementary geographic expression of the highest $^{3}He/^{4}He$ (northern hemisphere) and lowest $^{143}Nd/^{144}Nd$ (southern hemisphere) (Figure 8) highlights a possible mechanism influencing preservation of high $^{3}He/^{4}He$ in the mantle: that is, the magnitude of the highest $^{3}He/^{4}He$ signatures may be impacted by the geographic proximity to EM domains. Uranium and Th-rich continental crust is concentrated in the southern portions of the LLSVPs—in the continental crust-infused DUPAL domain positioned beneath the most extreme EM hotspots—and as a result, the associated excess ^{4}He produced by α-decay completely or partially overprints high-$^{3}He/^{4}He$ domains sampled by plumes upwelling from the DUPAL region. The ultra-high $^{3}He/^{4}He$ in the Iceland plume might be due to it being one of the northernmost hotspots, and therefore furthest away from the EM-infused DUPAL domain, which would make the Iceland mantle better preserved against mixing with low $^{3}He/^{4}He$ continental crust in the southern hemisphere.

This possible geographic (hemispheric) separation of the most geochemically enriched DUPAL domain in the southern hemisphere from the highest-$^{3}He/^{4}He$ (anti-DUPAL) domain in the northern hemisphere suggests that reservoir dynamics are not solely controlled by the density and/or viscosity of the primordial reservoir (Coltice et al., 2005; Dechamps et al., 2011; Gülcher et al., 2020; Samuel & Farnetani, 2003), but that geographic separation from addition of recycled continental crust is also important. The extraordinarily high U and Th concentrations (reflecting enrichment in incompatible trace elements) in continental crust, which are over an order of magnitude higher than in oceanic crust (Gale et al., 2013; Rudnick & Gao, 2003), will ultimately have a greater impact on the $^{3}He/^{4}He$ of primordial domains, and may help explain why the highest $^{3}He/^{4}He$ hotspot is furthest from the continental crust-rich DUPAL domain. This is consistent with the suggestion that the highest $^{3}He/^{4}He$ reservoir preserves its ancient noble gas signature because it is least influenced by subducted crustal materials (White, 2015).

5. Conclusions

EM type hotspots, which host recycled continental crust, are sourced by plumes originating in both Pacific and Indo-Atlantic LLSVPs, and the EM domains are concentrated in the southern hemisphere portions of both LLSVPs. EM signatures are not found in hotspots located outside of the margins of the LLSVPs. In contrast to EM, HIMU (which hosts recycled oceanic crust) is found both inside and outside of the LLSVPs.

The geographic decoupling of EM and HIMU is also explained if the LLSVPs have accumulated oceanic and continental crust over geologic time compared to regions outside of the LLSVPs, which is a result of downgoing slabs pushing subducted material into LLSVPs. As a result, there is less oceanic crust and continental crust outside the LLSVPs. Because much less continental crust is subducted than oceanic crust, there is far less continental crust than oceanic crust both outside and inside of the LLSVPs. Hence, continental crust is predicted to be scarce outside of the LLSVPs. It is possible that the amount of continental crust entrained and expressed as EM at hotspots is sufficiently low that continental crust entrainment in plumes is limited by the amount available. Therefore, EM is far more likely to be expressed in hotspots linked to the LLSVPs (where continental crust has accumulated) than outside the LLSVPs (where continental crust is scarce). In contrast, the amount of subducted oceanic crust is sufficiently abundant both inside and outside the LLSVPs that entrainment could be limited by the carrying capacity of the plume.

As a result, expressions of ancient recycled oceanic crust (i.e., HIMU) are identified in hotspots both inside and outside the LLSVPs.

While most high $^3He/^4He$ hotpots appear sourced from the LLSVPs, the plume conduit of the high $^3He/^4He$ Yellowstone hotspot is located far from LLSVPs, which indicates that the high $^3He/^4He$ reservoir is not restricted to the LLSVPs. While high $^3He/^4He$ is not well correlated with the LLSVPs, it is well correlated with hotspot buoyancy flux. Therefore, the example of Yellowstone suggests that an intrinsic property of a plume—its temperature and buoyancy flux, and therefore entrainment potential—governs whether a dense and possibly widespread (both inside and outside of the LLSVPs) high $^3He/^4He$ domain is entrained. Thus, the low frequency of high $^3He/^4He$ in hotspots outside of the LLSVPs is not evidence for paucity of high $^3He/^4He$ material outside of the LLSVPs, but instead relates to a paucity of high-buoyancy plumes outside of the LLSVPs capable of entraining a dense high $^3He/^4He$. Our reevaluation of hotspot feeding plume sources provides a baseline for future work linking plate tectonic and thermo-chemical convection models to the evolution of geochemical reservoirs.

Data Availability Statement

All data published in this manuscript are available in Jackson et al. (2020), Spatial characteristics of recycled and primordial reservoirs in the deep mantle, Version 1.0. Interdisciplinary Earth Data Alliance (IEDA). https://doi.org/10.26022/IEDA/111810.

Acknowledgments
We thank Bill White and Pat Castillo for constructive and helpful reviews. M. G. Jackson thanks Mark Kurz and Josh Curtice for providing helium measurements for the San Felix sample, and Sunna Harðardóttir for providing comments on the manuscript and helping to update the hotspot geochemical database. M. G. Jackson acknowledges support from National Science Foundation grants EAR-1900652, OCE-1928970 and OCE-1912931. T. W. Becker was supported by NSF EAR-1853856 and 1722680. B. Steinberger received support from the Research Council of Norway through its Centres of Excellence funding scheme, project number 223272, and additional funding from the innovation pool of the Helmholtz Association through the "Advanced Earth System Modeling Capacity (ESM)" activity. The Smithsonian National Museum of Natural History provided the San Felix lava with the generous support of Leslie Hale and Cathleen Brown.

References

Abedini, A. A., van Soest, M., Hurwitz, S., & Kennedy, B. M. (2006). Helium isotopes in basalt hosted olivines from the Yellowstone Plateau: implications on volcanic processes. Trans AGU EOS. Abstract V51D-1700.

Andrault, D., Bolfan-Casanova, N., Bouhifd, M. A., Boujibar, A., Garbarino, G., Manthilake, M., et al (2017). Toward a coherent model for the melting behavior of the deep Earth's mantle. *Physics of the Earth and Planetary Interiors*, *265*, 67–81.

Austermann, J., Kaye, B. T., Mitrovica, J. X., & Huybers, P. (2014). A statistical analysis of the correlation between Large Igneous Provinces and lower mantle seismic structure, *Geophysical Journal International*, *197*, 1–9. https://doi.org/10.1093/gji/ggt500

Ballmer, M. D., Houser, C., Hernlund, J. W., Wentzcovitch, R. M., & Hirose, K. (2017). Persistence of strong silica-enriched domains in the Earth's lower mantle. *Nature Geoscience*, *10*, 236–240.

Basu, A. R., Poreda, R. J., Renne, P. R., Teichmann, F., Vasiliev, Y. R., Sobolev, N. V., & Turrin, B. D. (1996). High-$^3He/^4He$ plume origin and temporal-spatial evolution of the Siberian flood basalts. *Science*, *269*, 822–825.

Becker, T. W., & Boschi, L. (2002). A comparison of tomographic and geodynamic mantle models. *Geochemistry, Geophysics, Geosystems*, *3*, 1003. https://doi.org/10.1029/2001GC000168

Becker, T. W., Kellogg, J. B., & O'Connell, R. J. (1999). Thermal constraints on the survival of primitive blobs in the lower mantle. *Earth and Planetary Science Letters*, *171*, 351–365.

Boschi, L., Becker, T. W., & Steinberger, B. (2007). Mantle plumes: Dynamic models and seismic images. *Geochemistry, Geophysics, Geosystems*, *7*, Q10006. https://doi.org/10.1029/2007GC001733

Boschi, L., Becker, T. W., & Steinberger, B. (2008). On the statistical significance of correlations between synthetic mantle plumes and tomographic models. *Physics of the Earth and Planetary Interiors*, *167*, 230–238.

Bouhifd, M. A., Jephcoat, A. P., Heber, V. S., & Kelley, S. P. (2013). Helium in Earth's early core. *Nature Geoscience*, *6*, 982–986.

Bouhifd, M. A., Jephcoat, A. P., Porcelli, D., Kelley, S. P., & Marty, B. (2020). Potential of Earth's core as a reservoir for noble gases: Case for helium and neon. *Geochemical Perspectives Letters*, *15*, 15–18. https://doi.org/10.7185/geochemlet.2028

Bouvier, A., Vervoort, J. D., & Patchett, P. J. (2008). The Lu–Hf and Sm–Nd isotopic composition of CHUR: Constraints from unequilibrated chondrites and implications for the bulk composition of terrestrial planets. *Earth and Planetary Science Letters*, *273*, 48–57.

Bower, D. J., Gurnis, M., & Seton, M. (2013). Lower mantle structure from paleogeographically constrained dynamic Earth models. *Geochemistry, Geophysics, Geosystems*, *14*, 44–63. https://doi.org/10.1029/2012GC004267

Broadley, M. W., Barry, P. H., Bekaert, D. V., Byrne, D. J., Caracausi, A., Ballentine, C. J., & Marty, B. (2020). Identification of chondritic krypton and xenon in Yellowstone gases and the timing of terrestrial volatile accretion. *Proceedings of the National Academy of Sciences*, *117*, 13997–14004.

Cabral, R. A., Jackson, M. G., Rose-Koga, E. F., Koga, K. T., Whitehouse, M. J., Antonelli, M. A., et al. (2013). Anomalous sulphur isotopes in plume lavas reveal deep mantle storage of Archaean crust. *Nature*, *496*, 490–493.

Castillo, P. R. (1988). The DUPAL anomaly as a trace of the upwelling lower mantle. *Nature*, *336*, 667–670.

Castillo, P. R. (2015). The recycling of marine carbonate and sources of HIMU and FOZO ocean island basalts. *Lithos*, *216–217*, 254–263.

Castillo, P. R., MacIsaac, C., Perry, S., & Veizer, J. (2018). Marine carbonates in the mantle source of oceanic basalts: Pb isotopic constraints. *Scientific Reports*, *8*, 14932. https://doi.org/10.1038/s41598-018-33178-4

Chauvel, C., Hofmann, A. W., & Vidal, P. (1992). HIMU-EM: The French Polynesian connection. *Earth and Planetary Science Letters*, *110*, 99–119.

Chiodini, G., Caliro, S., Lowenstern, J. B., Evans, W. C., Bergfeld, D., Tassi, F., & Tedesco, D. (2012). Insights from fumarole gas geochemistry on the origin of hydrothermal fluids on the Yellowstone Plateau. *Geochimica et Cosmochimica Acta*, *89*, 265–278.

Collerson, K. D., Williams, Q., Ewart, A. E., & Murphy, D. T. (2010). Origin of HIMU and EM-1 domains sampled by ocean island basalts, kimberlites and carbonatites: The role of CO_2-fluxed lower mantle melting in thermochemical upwellings. *Physics of the Earth and Planetary Interiors*, *181*, 112–131.

Coltice, N., Moreira, M., Hernlund, J., & Labrosse, S. (2005). Crystallization of a basal magma ocean recorded by helium and neon. *Earth and Planetary Science Letters*, *233*, 391–409.
Cottaar, S., & Romanowicz, B. (2012). An unusually large ULVZ at the base of the mantle near Hawaii. *Earth and Planetary Science Letters*, *355*, 213–222. https://doi.org/10.1016/j.epsl.2012.09.005
Courtillot, V., Davaille, A., Besse, J., & Stock, J. (2003). Three distinct types of hotspots in the Earth's mantle. *Earth and Planetary Science Letters*, *205*, 295–308.
Davaille, A. (1999). Simultaneous generation of hotspots and superswells by convection in a heterogeneous planetary mantle. *Nature*, *402*, 756–760.
Davaille, A., & Romanowicz, B. (2020), Deflating the LLSVPs: Bundles of mantle thermochemical plumes rather than thick stagnant "piles". *Tectonics*, *39*, e2020TC006265. https://doi.org/10.1029/2020TC006265
Davis, F. A., Hirschmann, M. M., & Humayun, M. (2011). The composition of the incipient partial melt of garnet peridotite at 3 GPa and the origin of OIB. *Earth and Planetary Science Letters*, 380–390.
Deschamps, F., Kaminski, E., & Tackley, P. J. (2011). A deep mantle origin for the primitive signature of ocean island basalt. *Nature Geoscience*, *4*, 879–882.
Domeier, M., Doubrovine, P. V., Gorsvik, T. H., Spakman, W., & Bull, A. (2016). Global correlation of lower mantle structure and past subduction. *Geophysical Research Letters*, *43*, 4945–4953. https://doi.org/10.1002/2016GL068827
Doucet, L. S., Li, Z.-X., El Dien, H. G., Pourteau, A., Murphy, J. B., Collins, W. J., et al. (2020). Distinct formation history for deep-mantle domains reflected in geochemical differences. *Nature Geoscience*, *13*, 511–515.
Dupré, B., & Allègre, C. J. (1983). Pb–Sr isotope variation in Indian Ocean basalts and mixing phenomena. *Nature*, *303*, 142–146.
Eisele, J., Sharma, M., Galer, S. J. G., Blichert-Toft, J., Devey, C. W., & Hofmann, A. W. (2002). The role of sediment recycling in EM-1 inferred from Os, Pb, Hf, Nd, Sr isotope and trace element systematics of the Pitcairn hotspot. *Earth and Planetary Science Letters*, *196*, 197–212.
French, S. W., & Romanowicz, B. (2015). Broad plumes rooted at the base of the Earth's mantle beneath major hotspots. *Nature*, *525*, 95–99.
Gale, A., Dalton, C. A., Langmuir, C. H., & Su, Y. (2013). The mean composition of ocean ridge basalts. *Geochemistry, Geophysics, Geosystems*, *14*, 489–518. https://doi.org/10.1029/2012GC004334
Galer, S. J. G., & O'Nions, R. K. (1985). Residence time of thorium, uranium, and lead in the mantle with implications for mantle convection. *Nature*, *316*, 778–782.
Graham, D. W. (2002). Noble gas isotope geochemistry of mid-ocean ridge and ocean island basalts: characterization of mantle source reservoirs. In D. Porcelli, C. J. Ballentine, & R. Wieler (Eds.), *Noble gases in geochemistry and cosmochemistry* (pp. 247–318). Mineralogical Society of America.
Graham, D. W., Reid, M. R., Jordan, B. T., Grunder, A. L., Leeman, W. P., & Lupton, J. E. (2009). Mantle source provinces beneath the Northwestern USA delimited by helium isotopes in young basalts. *Journal of Volcanology and Geothermal Research*, *188*, 128–140.
Gülcher, A. J. P., Gebhardt, D. J., Ballmer, M. D., & Tackley, P. J. (2020). Variable dynamic styles of primordial heterogeneity preservation in the Earth's lower mantle. *Earth and Planetary Science Letters*, *536*, 116160.
Hager, B. H., Clayton, R. W., Richards, M. A., Comer, R. P., & Dziewonski, A. M. (1985). Lower mantle heterogeneity, dynamic topography, and the geoid. *Nature*, *313*, 541–545.
Hanyu, T., & Kaneoka, I. (1997). The uniform and low $^{3}He/^{4}He$ ratios of HIMU basalts as evidence for their origin as recycled materials. *Nature*, *390*, 273–276.
Hanyu, T., Tatsumi, Y., Senda, R., Miyazaki, T., Chang, Q., Hirahara, Y., et al. (2011). Geochemical characteristics and origin of the HIMU reservoir: A possible mantle plume source in the lower mantle. *Geochemistry, Geophysics, Geosystems*, *12*, Q0AC09. https://doi.org/10.1029/2010GC003252
Hart, S. R. (1984). A large-scale isotope anomaly in the Southern Hemisphere mantle. *Nature*, *309*, 753–757.
Hauri, E. H., & Hart, S. R. (1993). Re-Os isotope systematics of HIMU and EMII oceanic island basalts from the south Pacific Ocean. *Earth and Planetary Science Letters*, *114*, 353–371.
Hofmann, A. W. (2014), Sampling mantle heterogeneity through oceanic basalts: isotopes and trace elements. *Treatise on Geochemistry*, *3*, 67–101.
Hofmann, A. W., & White, W. M. (1982). Mantle plumes from ancient oceanic crust. *Earth and Planetary Science Letters*, *57*, 421–436.
Horan, M. F., Carlson, R. W., Walker, R. J., Jackson, M. G., Garçon, M., & Norman, M. (2018). Tracking Hadean processes in modern basalts. *Earth and Planetary Science Letters*, *484*, 184–191.
Ionov, D. A., Doucet, L. S., Carlson, R. W., Golovin, A. V., & Korsakov, A. V. (2015). Post-Archean formation of the lithospheric mantle in the central Siberian craton: Re-Os and PGE study of peridotite xenoliths from the Udachnaya kimberlite. *Geochimica et Cosmochimica Acta*, *165*, 466–483.
Jackson, M. G., Becker, T., & Konter, J. G. (2018a). Evidence for a deep mantle source for EM and HIMU domains from integrated geochemical and geophysical constraints. *Earth and Planetary Science Letters*, *484*, 1–14.
Jackson, M. G., Becker, T. W., & Konter, J. G. (2018b). Geochemistry and distribution of recycled domains in the mantle inferred from Nd and Pb isotopes in oceanic hotspots: implications for storage in the large low shear wave velocity provinces (LLSVPs). *Geochemistry, Geophysics, Geosystems*, *19*, 3496–3519. https://doi.org/10.1029/2018GC007552
Jackson, M. G., Hart, S. R., Koppers, A. A. P., Staudigel, H., Konter, J., Blusztajn, J., et al. (2007a). The return of subducted continental crust in Samoan lavas. *Nature*, *448*, 684–687.
Jackson, M. G., Konter, J. G., & Becker, T. W. (2017). Primordial helium entrained by the hottest mantle plumes. *Nature*, *542*, 340–343.
Jackson, M. G., Kurz, M. D., Hart, S. R., & Workman, R. K. (2007b). New Samoan lavas from Ofu Island reveal a hemispherically heterogeneous high $^{3}He/^{4}He$ mantle. *Earth and Planetary Science Letters*, *264*, 360–374.
Jellinek, A. M., & Manga, M. (2004). Links between long-lived hotspots, mantle plume, D′′, and plate tectonics. *Reviews of Geophysics*, *42*, RG3002.
Kendrick, M. A., Hémond, C., Kamenetsky, V. S., Danyushevsky, L., Devey, C. W., Rodemann, T., et al. (2017). Seawater cycled throughout Earth's mantle in partially serpentinized lithosphere. *Nature Geoscience*, *10*, 222–228.
Kim, D., Lekić, V., Ménard, B., Baron, D., & Taghizadeh-Popp, M. (2020). Sequencing seismograms: A panoptic view of scattering in the core-mantle boundary region. *Science*, *368*, 1223–1228.
Konter, J. G., & Becker, T. W. (2012). Shallow lithospheric contribution to mantle plumes revealed by integrating seismic and geochemical data, *Geochemistry, Geophysics, Geosystems*, *13*, Q02004. https://doi.org/10.1029/2011GC003923
Kurz, M. D., Jenkins, W. J., & Hart, S. R. (1982). Helium isotopic systematics of oceanic islands and mantle heterogeneity. *Nature*, *297*, 43–47.

Labidi, J., Barry, P. H., Bekaert, D. V., Broadley, M. W., Marty, B., Giunta, T., et al. (2020). Hydrothermal $^{15}N^{15}N$ abundances constrain the origins of mantle nitrogen. *Nature*, *580*, 367–371.
Licciardi, J. M., Clark, P. U., Brook, E. J., Pierce, K. L., Kurz, M. D., Elmore, D., & Sharma, P. (2001). Cosmogenic ^{3}He and ^{10}Be chronologies of the late Pinedale northern Yellowstone ice cap, Montana, USA. *Geology*, *29*, 1095–1098.
Lin, S.-C., & van Keken, P. E. (2006). Dynamics of thermochemical plumes: 2. Complexity of plume structures and its implications for mapping mantle plumes. *Geochemistry, Geophysics, Geosystems*, *7*, Q03003. https://doi.org/10.1029/2005GC001072
Lowenstern, J. B., Evans, W. C., Bergfeld, D., & Hunt, A. G. (2014). Prodigious degassing of a billion years of accumulated radiogenic helium at Yellowstone. *Nature*, *506*, 355–358.
Lu, C., & Grand, S. P. (2016). The effect of subducting slabs in global shear wave tomography. *Geophysical Journal International*, *205*, 1074–1085.
Macpherson, C. G., Hilton, D. R., Sinton, J. M., Poreda, R. J., & Craig, H. (1998). High $^{3}He/^{4}He$ ratios in the Manus backarc basin: Implications for mantle mixing and the origin of plumes in the western Pacific Ocean. *Geology*, *26*, 1007–1010.
Marignier, A., Ferreira, A. M. G., & Kitching, T. (2020). The probability of mantle plumes in global tomographic models. *Geochemistry, Geophysics, Geosystems*, *21*, e2020GC009276. https://doi.org/10.1029/2020GC009276
Mazza, S. E., Gazel, E., Bizimis, M., Moucha, R., Béguelin, P., Johnson, E. A., et al. (2019). Sampling the volatile-rich transition zone beneath Bermuda. *Nature*, *569*, 398–403.
McNamara, A. K., & Zhong, S. (2004). Thermochemical structures within a spherical mantle: Superplumes or piles? *Journal of Geophysical Research: Solid Earth*, *109*(B7), B07402. https://doi.org/10.1029/2003JB002847
McNamara, A. K., & Zhong, S. (2005). Thermochemical structures beneath Africa and the Pacific Ocean. *Nature*, *437*, 1136–1139.
Mukhopadhyay, S. (2012). Early differentiation and volatile accretion recorded in deep-mantle neon and xenon. *Nature*, *486*, 101–104.
Mundl-Petermeier, A., Walker, R. J., Fischer, R. A., Lekić, V., Jackson, M. G., & Kurz, M. D. (2020). Anomalous ^{182}W in high $^{3}He/^{4}He$ Ocean Island Basalts: Fingerprints of Earth's core? *Geochimica et Cosmochimica Acta*, *271*, 194–211.
Mundl, A., Touboul, M., Jackson, M. G., Day, J. M. D., Kurz, M. D., Lekić, V., et al. (2017). Tungsten-182 heterogeneity in modern ocean island basalts. *Science*, *356*, 66–69.
Nelson, P. L., & Grand, S. P. (2018). Lower-mantle plume beneath the Yellowstone hotspot revealed by core waves. *Nature Geoscience*, *11*, 280–284.
Peters, B. J., Carlson, R. W., Day, J. M. D., & Horan, M. F. (2018). Hadean silicate differentiation preserved by anomalous $^{142}Nd/^{144}Nd$ ratios in the Réunion hotspot source. *Nature*, *555*, 89–93.
Pilet, S., Baker, M. B., & Stolper, E. M. (2008). Metasomatized lithosphere and the origin of alkaline lavas. *Science*, *320*, 916–919.
Porcelli, D., & Halliday, A. N. (2001). The core as a possible source of mantle helium. *Earth and Planetary Science Letters*, *192*, 45–56.
Prytulak, J., & Elliott, T. (2007). TiO_2 enrichment in ocean island basalts. *Earth and Planetary Science Letters*, *263*, 388–403.
Putirka, K. (2008). Excess temperatures at ocean islands: implications for mantle layering and convection. *Geology*, *36*, 283–286.
Richards, M. A., Hager, B. H., & Sleep, N. H. (1988). Dynamically supported geoid highs over hotspots: Observation and theory. *Journal of Geophysics Research*, *93*, 7690–7708. https://doi.org/10.1029/JB093iB07p07690
Ritsema, J., Deuss, A., van Heijst, J. J., & Woodhouse, J. H. (2011). S40RTS: A degree-40 shear-velocity model for the mantle from new Rayleigh wave dispersion, teleseismic traveltime and normal-mode splitting function measurements. *Geophysical Journal International*, *184*, 1223–1236.
Rizo, H., Andrault, D., Bennett, N. R., Humayun, M., Brandon, A., Vlastelic, I., et al. (2019). ^{182}W evidence for core-mantle interaction in the source of mantle plumes. *Geochemical Perspectives Letters*, *11*, 6–11. https://doi.org/10.7185/geochemlet.1917
Rudnick, R. L., & Gao, S. (2003). Composition of the continental crust. In R. L. Rudnick (Ed.), *Treatise on geochemistry, the crust* (pp. 1–64). Elsevier.
Samuel, H., & Farnetani, C. G. (2003). Thermochemical convection and helium concentrations in mantle plumes. *Earth and Planetary Science Letters*, *207*, 39–56.
Schubert, G., Masters, G., Olson, P., & Tackley, P. (2004). Superplumes or plume clusters? *Physics of the Earth and Planetary Interiors*, *146*, 147–162.
Starkey, N. A., Stuart, F. M., Ellam, R. M., Fitton, J. G., Basu, S., & Larsen, L. M. (2009). Helium isotopes in early Iceland plume picrites: Constraints on the composition of high $^{3}He/^{4}He$ mantle. *Earth and Planetary Science Letters*, *277*, 91–100.
Steinberger, B., & Calderwood, A. R. (2006). Models of large-scale viscous flow in the Earth's mantle with constraints from mineral physics and surface observations. *Geophysical Journal International*, *167*, 1461–1481.
Steinberger, B., Nelson, P. L., Grand, S. P., & Wang, W. (2019). Yellowstone plume conduit tilt caused by large-scale mantle flow. *Geochemistry, Geophysics, Geosystems*, *20*, 5896–5912. https://doi.org/10.1029/2019gc008490
Steinberger, B., & O'Connell, R. J. (1998). Advection of plumes in mantle flow; implications on hotspot motion, mantle viscosity and plume distribution. *Geophysical Journal International*, *132*, 412–434.
Steinberger, B., & Torsvik, T. H. (2012). A geodynamic model of plumes from the margins of Large Low Shear Velocity Provinces. *Geochemistry, Geophysics, Geosystems*, *13*, Q01W09. https://doi.org/10.1029/2011GC003808
Stracke, A. (2012). Earth's heterogeneous mantle: A product of convection-driven interaction between crust and mantle. *Chemical Geology*, *330–331*, 274–299.
Tan, E., Gurnis, M., & Han, L. (2002). Slabs in the lower mantle and their modulation of plume formation. *Geochemistry, Geophysics, Geosystems*, *3*, 1067. https://doi.org/10.1029/2001GC000238
Thorne, M. S., Garnero, E. J., & Grand, S. (2004). Geographic correlation between hot spots and deep mantle lateral shear-wave velocity gradients. *Physics of the Earth and Planetary Interiors*, *146*, 47–63.
Thorne, M. S., Garnero, E. J., Jahnke, G., Igel, H., & McNamara, A. K. (2013). Mega ultra low velocity zone and mantle flow. *Earth and Planetary Science Letters*, *364*, 59–67. https://doi.org/10.1016/j.epsl.2012.12.034
Torsvik, T. H., Smethurst, M. A., Burke, K., & Steinberger, B. (2006). Large igneous provinces generated from the margins of the large low velocity provinces in the deep mantle. *Geophysical Journal International*, *167*, 1447–1460.
Torsvik, T. H., Steinberger, B., Cocks, L. R. M., & Burke, K. (2008). Longitude: Linking Earth's ancient surface to its deep interior, *Earth and Planetary Science Letters*, *276*, 273–282, https://doi.org/10.1016/j.epsl.2008.09.026
Torsvik, T. H., Svensen, H. H., Steinberger, B., Royer, D. L., Jerram, D. A., Jones, M. T., & Domeier, M., (in press). Connecting the deep Earth and the atmosphere. In H. Marquardt, S. Cottaar, J. Konter, & M. Ballmer (Eds.), *Mantle convection and surface expressions*. Washington, DC: AGU. https://eartharxiv.org/25a9c
Van der Meer, D., Spakman, W., van Hinsbergen, D. J. J., Amaru, M. L., & Torsvik, T. H. (2010). Towards absolute plate motions constrained by lower-mantle slab remnants. *Nature Geoscience*, *3*, 36–40.

Weis, D., Garcia, M. O., Rhodes, J. M., Jellinek, M., & Scoates, J. S. (2011). Role of the deep mantle in generating the compositional asymmetry of the Hawaiian mantle plume. *Nature Geoscience*, *4*, 831–838.
Weiss, Y., Class, C., Goldstein, S. L., & Hanyu, T. (2016). Key new pieces of the HIMU puzzle from olivines and diamond inclusions. *Nature*, *537*, 666–670.
White, W. M. (2015). Isotopes, DUPAL, LLSVPs, and Anekantavada. *Chemical Geology*, *419*, 10–28.
White, W. M., & Hofmann, A. W. (1982). Sr and Nd isotope geochemistry of oceanic basalts and mantle evolution. *Nature*, *296*, 821–825.
Williams, C. D., Mukhopadhyay, S., Rudolph, M. L., & Romanowicz, B. (2019). Primitive helium is sourced from seismically slow regions in the lowermost mantle. *Geochemistry, Geophysics, Geosystems*, *20*, 4130–4145.
Williams, Q., & Garnero, E. J. (1996). Seismic evidence for partial melt at the base of Earth's mantle. *Science*, *273*, 1528–1530.
Williams, Q., Revenaugh, J., & Garnero, E. (1998). A correlation between ultra-low basal velocities in the mantle and hot spots. *Science*, *281*, 546–549.
Yanagisawa, T., & Hamano, Y. (1999). "Skewness" of S-wave velocity in the mantle. *Geophysical Research Letters*, *26*, 791–794.
Yu, S., & Garnero, E. J. (2018). Ultra-low velocity zone locations: A global assessment. *Geochemistry, Geophysics, Geosystems*, *19*, 396–414. https://doi.org/10.1002/2017GC007281
Yuan, K. Q., & Romanowicz, B. (2017). Seismic evidence for partial melting at the root of major hot spot plumes. *Science*, *357*, 393–396.
Zhang, N., Zhong, S., Leng, W., & Li, Z. -X. (2010). A model for the evolution of the Earth's mantle structure since the Early Paleozoic. *Journal of Geophysical Research*, *115*, B06401. https://doi.org/10.1029/2009JB006896
Zhong, S., Zhang, N., Li, Z.-X., & Roberts, J. H. (2007). Supercontinent cycles, true polar wander, and very long-wavelength mantle convection. *Earth and Planetary Science Letters*, *261*, 551–564.

References From the Supporting Information

Aka, F. T., Nagao, K., Kusakabe, M., Sumino, H., Tanyileke, G., Atemba, B., & Hell, J. (2004). Symmetrical helium isotope distribution on the Cameroon volcanic line, West Africa. *Chemical Geology*, *203*, 205–223.
Albers, M., & Christensen, U. R. (1996). The excess temperature of plumes rising from the core-mantle boundary. *Geophysical Research Letters*, *23*, 3567–3570.
Ammon, K., Dunai, T. J., Stuart, F. M., Meriaux, A.-S., & Gayer, E. (2009). Cosmogenic ^{3}He exposure ages and geochemistry of basalts from Ascension Island, Atlantic Ocean. *Quaternary Geochronology*, *4*, 525–532.
Auer, L., Boschi, L., Becker, T. W., Nissen-Meyer, T., & Giardini, D. (2014). Savani: A variable-resolution whole-mantle model of anisotropic shear-velocity variations based on multiple datasets. *Journal of Geophysical Research*, *119*, 3006–3034. https://doi.org/10.1002/2013JB010773
Barling, J., Goldstein, S. L., & Nicholls, I. A. (1994). Geochemistry of Heard Island (Southern Indian Ocean): Characterization of an enriched mantle component and implications for enrichment of the sub-Indian Ocean mantle. *Journal of Petrology*, *35*, 1017–1053.
Barry, T. L., Pearce, J. A., Leat, P. T., Millar, I. L., & Le Roex, A. P. (2006). Hf isotope evidence for selective mobility of high-field-strength elements in a subduction setting: South Sandwich Islands. *Earth and Planetary Science Letters*, *252*, 223–244.
Becker, T. W., & Boschi, L. (2002). A comparison of tomographic and geodynamic mantle models. *Geochemistry, Geophysics, Geosystems*, *3*, 1003. https://doi.org/10.1029/2001GC000168
Bohrson, W. A., & Reid, M. R. (1995). Petrogenesis of alkaline basalts from Socorro Island, Mexico: Trace element evidence for contamination of ocean island basalts in the shallow ocean crust. *Journal of Geophysical Research*, *B100*, 24555–24576.
Bonneville, A., Dosso, L., & Hildebrand, A. (2006). Temporal evolution and geochemical variability of the South Pacific superplume activity. *Earth and Planetary Science Letters*, *224*, 251–269.
Bosch, D., Blichert-Toft, J., Moynier, F., Nelson, B. K., Telouk, P., Gillot, P.-Y., & Albarède, F. (2008). Pb, Hf, and Nd isotope compositions of the two Reunion volcanoes (Indian Ocean): A tale of two small-scala mantle "blobs"? *Earth and Planetary Science Letters*, *265*, 748–768.
Boschi, L., Becker, T. W., & Steinberger, B. (2007). Mantle plumes: Dynamic models and seismic images. *Geochemistry, Geophysics, Geosystems*, *7*, Q10006.
Brenton, T., Nauret, F., Pichat, S., Moine, B. N., Moreira, M. A., Rose-Koga, E. F., et al. (2013). Geochemical heterogeneities within the Crozet hotspot. *Earth and Planetary Science Letters*, *376*, 126–136.
Castillo, P. R., Scarsi, P., & Craig, H. (2007). He, Sr, Nd and Pb isotopic constraints on the origin of the Marquesas and other linear volcanic chains. *Chemical Geology*, *240*, 205–221.
Chadwick, J. P., Keller, R. A., Kamenov, G. D., Yogodzinski, G. M., & Lupton, J. E. (2014). The Cobb hotspot: HIMU-DMM mixing and melting controlled by a progressively thinning lithospheric lid. *Geochemistry, Geophysics, Geosystems*, *15*, 3107–3122. https://doi.org/10.1002/2014GC005334
Chang, S.-J., Kendall, E., Davaille, A., & Ferreira, A. M. G. (2020). The evolution of mantle plumes in East Africa. *Journal of Geophysical Research: Solid Earth*, *125*, e2020JB019929. https://doi.org/10.1029/2020JB019929
Chu-Yung, C., Frey, F. A., Rhodes, J. M., & Easton, R. M. (1996). *Temporal geochemical evolution of Kilauea volcano: Comparison of Hilina and Puna basalt*. In A. Basu, & S. R. Hart (Eds.), Earth processes, reading the isotopic code (pp. 161–181). Washington DC: AGU.
Class, C., Goldstein, S. L., Stute, M., Kurz, M. D., & Schlosser, P. (2005). Grand Comore Island: A well-constrained low ^{3}He/^{4}He mantle plume. *Earth and Planetary Science Letters*, *233*, 391–409.
Cohen, R. S., & O'Nions, R. K. (1982). Identification of recycled continental material in the mantle from Sr, Nd and Pb isotope investigations. *Earth and Planetary Science Letters*, *61*, 73–84.
Cordier, C., Chauvel, C., & Hémond, C. (2016). High-precision lead isotopes and stripy plumes: revisiting the Society chain in French Polynesia. *Geochimica et Cosmochimica Acta*, *189*, 236–250.
Davies, G. F. (1988). Ocean bathymetry and mantle convection 1. Large-scale flow and hotspots. *Journal of Geophysical Research*, *93*, 10467–10480.
Davies, G. F. (1992). Temporal variation of the Hawaiian plume flux. *Earth and Planetary Science Letters*, *113*, 277–286.
Day, J. M. D., & Hilton, D. R. (2011). Origin of ^{3}He/^{4}He ratios in HIMU-type basalt constrained from Canary Island lavas. *Earth and Planetary Science Letters*, *305*, 226–234.
Desonie, D. L., Duncan, R. A., & Natland, J. H. (1993). Temporal and geochemical variability of volcanic products of the Marquesas hotspot. *Journal of Geophysical Research*, *B98*, 17649–17665.

Doucelance, R., Escrib, S., Moreira, M., Gariepy, C., & Kurz, M. D. (2003). Pb-Sr-He isotope and trace element geochemistry of the Cape Verde archipelago. *Geochimica et Cosmochimica Acta*, *67*, 3717–3733.
Dunai, T. J., & Baur, H. (1995). Helium, neon, and argon systematics of the European subcontinental mantle: Implications for its geochemical evolution. *Geochimica et Cosmochimica Acta*, *59*, 2767–2783.
Dupuy, C., Vidal, P., Maury, R. C., & Guille, G. (1993). Basalts from Mururoa, Fangataufa, and Gambier islands (French Polynesia): Geochemical dependence on the age of the lithosphere. *Earth and Planetary Science Letters*, *117*, 89–100.
Eggins, S. M., Green, D. H., & Falloon, T. J. (1991). The Tasmantid seamounts: Shallow melting and contamination of an EM1 mantle plume. *Earth and Planetary Science Letters*, *107*, 448–462.
Eiler, J. M., Farley, K. A., Valley, J. W., Hauri, E., Craig, H., Hart, S. R., & Stolper, E. M. (1997). Oxygen isotope variations in ocean island basalt phenocrysts. *Geochimica et Cosmochimica Acta*, *61*, 2281–2293.
Eisele, J., Sharma, M., Galer, S. J. G., Blichert-Toft, J., Devey, C. W., & Hofmann, A. W. (2002). The role of sediment recycling in EM-1 inferred from Os, Pb, Hf, Nd, Sr isotope and trace element systematics of the Pitcairn hotspot. *Earth and Planetary Science Letters*, *196*, 197–212.
Elkins, L. J., Hamelin, C., Blichert-Toft, J., Scott, S. R., Sims, K. W. W., Yeo, I. A., et al. (2016). North Atlantic hotspot-ridge interaction near Jan Mayen Island. *Geochemical Perspective Letters*, *2*, 55–67.
Farley, K. A., Basu, A. R., & Craig, H. (1993). He, Sr, and Nd isotopic variations in lavas from Juan Fernandez archipelago, SE Pacific. *Contributions to Mineralogy and Petrology*, *115*, 75–87.
Franz, G., Steiner, G., Volker, F., & Pudlo, D. (1999). Plume related alkaline magmatism in Central Africa – the Meidob Hills (W. Sudan). *Chemical Geology*, *157*, 27–47.
Garapic, G., Jackson, M. G., Hauri, E. H., Hart, S. R., Farley, K. A., Blusztajn, J. S., & Woodhead, J. D. (2015). A radiogenic isotopic (He-Sr-Nd-Pb-Os) study of the lavas from the Pitcairn hotspot: implications for the origin of the EM-1 (enriched mantle 1). *Lithos*, *228–229*, 1–11.
Geldmacher, J., Hoernle, K., Bogaard, P. v.d., Dugen, S., & Werner, R. (2005). New $^{40}Ar/^{39}Ar$ age and geochemical data from seamounts in the Canary and Madeira volcanic province: support for the mantle plume hypothesis. *Earth and Planetary Science Letters*, *237*, 85–101.
Gerlach, D. C., Cliff, R. A., Davies, G. R., Norry, M. J., & Hodgson, N. (1988). Magma source of the Cape Verdes archipelago: isotopic and trace element constraints. *Geochimica et Cosmochimica Acta*, *52*, 2979–2992.
Gerlach, D. C., Hart, S. R., Morales, V. W. J., & Palacios, C. (1986). Mantle heterogeneity beneath the Nazca plate: San Felix and Juan Fernandez Islands. *Nature*, *322*, 165–169.
Gerlach, D. C., Stormer, J. C., Jr, & Mueller, P. A. (1987). Isotopic geochemistry of Fernando de Noronha. *Earth and Planetary Science Letters*, *85*, 129–144.
Graham, D. W., Johnson, K. T. M., Priebe, L. D., & Lupton, J. E. (1999). Hotspot-ridge interaction along the Southeast Indian Ridge near Amsterdam and St. Paul Islands: Helium isotope evidence. *Earth and Planetary Science Letters*, *167*, 297–310.
Graham, D. W., Lupton, J., Alberède, F., & Condomines, M. (1990). Extreme temporal homogeneity of helium isotopes at Piton de la Fornaise, Reunion Island. *Nature*, *347*, 545–548.
Graham, D. W., Reid, M. R., Jordan, B. T., Grunder, A. L., Leeman, W. P., & Lupton, J. E. (2009). Mantle source provinces beneath the northwestern USA delimited by helium isotopes in young basalts. *Journal of Volcanology and Geothermal Research*, *188*, 128–140.
Gurenko, A. A., Hoernle, K. A., Hauff, F., Schmincke, H.-U., Han, D., Miura, Y. N., & Kaneoka, I. (2006). Major, trace element and Nd-Sr-Pb-O-He-Ar isotope signatures of shield stage lavas from the central and western Canary Islands: Insights into mantle and crustal processes. *Chemical Geology*, *223*, 75–112.
Halliday, A. N., Davidson, J. P., Holden, P., DeWolf, C., Lee, D.-C., & Fitton, J. G. (1990). Trace-element fractionation in plumes and the origin of HIMU mantle beneath the Cameroon Line. *Nature*, *347*, 523–528.
Halliday, A. N., G. R. Davies, D.-C. Lee, S. Tommasini, C. R. Paslick, J. G. Fitton, & James, D. E. (1992). Lead isotope evidence for young trace element enrichment in the oceanic upper mantle. *Nature*, *359*, 623–627.
Hamelin, B., Dupré, B., & Allègre, C.-J. (1986). Pb-Sr-Nd isotopic data on Indian Ocean ridges: New evidence of large-scale mapping of mantle heterogeneities. *Earth and Planetary Science Letters*, *76*, 288–298.
Hanyu, T. (2014). Deep plume origin of the Louisville hotspot: Noble gas evidence. *Geochemistry, Geophysics, Geosystems*, *15*, 565–576.
Hanyu, T., Kawabata, H., Tatsumi, Y., Kimura, J.-I., Hyodo, H., Sato, K., et al. (2014). Isotope evolution in the HIMU reservoir beneath St. Helena: Implications for the mantle recycling of U and Th. *Geochimica et Cosmochimica Acta*, *143*, 232–252.
Hanyu, T., & Kaneoka, I. (1997). The uniform and low $^{3}He/^{4}He$ ratios of HIMU basalts as evidence for their origin as recycled materials. *Nature*, *390*, 273–276.
Hanyu, T., Tatsumi, Y., Senda, R., Miyazaki, T., Chang, Q., Hirahara, Y., et al. (2011). Geochemical characteristics and origin of the HIMU reservoir: A possible mantle plume source in the lower mantle. *Geochemistry, Geophysics, Geosystems*, *12*, Q0A09. https://doi.org/10.1029/2010GC003252
Harpp, K. S., & White, W. M. (2000). Tracing a mantle plume: isotopic and trace element variations of Galapagos seamounts. *Geochemistry, Geophysics, Geosystems*, *2*, 1042, https://doi.org/10.1029/2000GC000137
Harpp, K. S., Geist, D., Koleszar, A. M., Christensen, B., Lyons, J., Sabga, M., & Rollins, N. (2014). The geology and geochemistry of Isla Floreana, Galapagos: A different type of late-stage ocean island volcanism. In K. Harpp, E. Mittlestaedt, D. Graham, & N. D'Ozouville (Eds.), *The Galapagos: A natural Laboratory for the Earth Sciences*. Washington: DC: American Geophysical Union.
Hart, S. R. (1984). A large-scale isotope anomaly in the Southern Hemisphere mantle. *Nature*, *309*, 753–757.
Hart, S. R. (1988). Heterogeneous mantle domains: signatures, genesis, and mixing chronologies. *Earth and Planetary Science Letters*, *90*, 273–296.
Hegner, E., & Tatsumoto, M. (1989). Pb, Sr and Nd isotopes in seamount basalts from the Juan de Fuca Ridge and Kodiak-Bowie seamount chain, Northeast Pacific. *Journal of Geophysical Research*, *94*, 17839–17846.
Hilton, D. R., Barling, J., & Wheller, G. E. (1995). Effect of shallow-level contamination on the helium isotope systematics of ocean-island lavas. *Nature*, *373*, 330–333.
Hilton, D. R., Halldórsson, S. A., Barry, P. H., Fischer, T. P., de Moor, J. M., Ramirez, C. J., et al. (2011). Helium isotopes in Rungwe Volcanic Province, Tanzania, and the origin of the East African Plateaux. *Geophysical Research Letters*, *38*, L21304. https://doi.org/10.1029/2011GL049589
Hoernle, K., Rohde, J., Hauff, F., Garbe-Schönberg, D., Homrighausen, S., Werner, R., & Morgan, J. P. (2015). How and when plume zonation appeared during the 132 Myr evolution of the Tristan hotspot. *Nature Communications 6*, 7799. https://doi.org/10.1038/ncomms8799

Hoernle, K., Schwindrofska, A., Werner, R., van den Bogaard, P., Hauff, F., Uenzelmann-Neben, G., & Garbe-Schönberg, D. (2016). Tectonic dissection and displacement of parts of Shona hotspot volcano 3500 km along the Agulhas-Falkland Fracture Zone. *Geology*, *44*, 263–266.

Hoggard, M. J., Parnell-Turner, R., & White, N. (2020). Hotspots and mantle plumes revisited: Toward reconciling the mantle heat transfer discrepancy. *Earth and Planetary Science Letters*, *542*, 116317. https://doi.org/10.1016/j.epsl.2020.116317

Ito, G., Lin, J., & Gable, C. W. (1997). Interaction of mantle plumes and migrating mid-ocean ridges: Implications for the Galápagos plume-ridge system. *Journal of Geophysical Research*, *102*(B7), 15403–15417. https://doi.org/10.1029/97JB01049

Jackson, M. G., Hart, S. R., Konter, J. G., Koppers, A. A. P., Kurz, M. D., Blusztajn, J. M., & Sinton, J. M. (2010). The Samoan hotspot on a "hotspot highway": implication for mantle plumes and a deep Samoan mantle source. *Geochemistry, Geophysics, Geosystems*, *11*, Q12009. https://doi.org/10.1029/2010GC003232

Jackson, M. G., Hart, S. R., Koppers, A. A. P., Staudigel, H., Konter, J., Blusztajn, J., et al. (2007). The return of subducted continental crust in Samoan lavas. *Nature*, *448*, 684–687.

Jackson, M. G., Hart, S. R., Saal, A. E., Shimizu, N., Kurz, M. D., Blusztajn, J. S., & Skovgaard, A. C. (2008). Globally elevated titanium, tantalum, and niobium (TITAN) in ocean island basalts with high $^{3}He/^{4}He$. *Geochemistry, Geophysics, Geosystems*, *9*, Q04027. https://doi.org/10.1029/2007GC001876

Jackson, MG., Kurz, M. D., Hart, S. R., & Workman, R. (2007). New Samoan lavas from Ofu Island reveal a hemispherically heterogeneous high $^{3}He/^{4}He$ mantle. *Earth and Planetary Science Letters*, *264*, 360–374.

Jackson, M. G., Price, A. A., Blichert-Toft, J., Kurz, M. D., & Reinhard, A. A. (2017a). Geochemistry of lavas from the Caroline hotspot, Micronesia: evidence from primitive and recycled components in the mantle sources of lavas from moderately elevated $^{3}He/^{4}He$. *Chemical Geology*, *455*, 385–400.

Jackson, M. G., Konter, J. G., & Becker, T. W. (2017b). Primordial helium entrained by the hottest mantle plumes. *Nature*, *542*, 340–343.

Jackson, M. G., Becker, T., & Konter, J. G. (2018a). Evidence for a deep mantle source for EM and HIMU domains from integrated geochemical and geophysical constraints. *Earth and Planetary Science Letters*, *484*, 1–14.

Jackson, M. G., Becker, T. W., & Konter, J. G. (2018b). Geochemistry and distribution of recycled domains in the mantle inferred from Nd and Pb isotopes in oceanic hotspots: implications for storage in the large low shear wave velocity provinces (LLSVPs). *Geochemistry, Geophysics, Geosystems*, *19*, 3496–3519. https://doi.org/10.1029/2018GC007552

Jackson, M. G., Blichert-Toft, J., Halldórsson, S. A., Mundl-Petermeier, A., Bizimis, M., Kurz, M. D., et al. (2020). Ancient He and W isotopic signatures preserved in mantle domains least modified by crustal recycling. *Proceedings of the National Academy of Sciences*, *117*, 30993–31001.

Kendrick, M. A., Hémond, C., Kamenetsky, V. S., Danyushevsky, L., Devey, C., Rodemann, T., et al. (2017). Seawater cycled throughout Earth's mantle in partially serpentinized lithosphere. *Nature Geoscience*, *10*, 222–228.

King, S. D., & Adam, C. (2014). Hotspot swells revisited. *Physics Earth Planet Int*, *235*, 66–83.

Kingsley, R. H., & Schilling, J.-G. (1998). Plume-ridge interaction in the Easter-Salas y Gomez seamount chain – Easter Microplate system: Pb isotope evidence. *Journal of Geophysical Research*, *B103*, 24159–24177.

Kingsley, R. H., Blichert-Toft, J., Fontignie, D., & Schilling, J.-G. (2007). Hafnium, neodymium, and strontium isotope and parent daughter element systematics in basalts from the plume-ridge interaction system of the Salas y Gomes seamount chain and the Easter Microplate. *Geochemistry, Geophysics, Geosystems*, *8*, Q04005. https://doi.org/10.1029/2006GC001401

Kokfelt, T. F., Hoernle, K. A., Hauff, F., Fiebig, J., Werner, R., & Garbe-Schönberg, D. (2006). Combined trace element and Pb-Nd-Sr-O isotope evidence for recycled oceanic crust (upper and lower) in the Iceland mantle plume. *Journal of Petrology*, *47*, 1705–1749.

Konter, J. G., Staudigel, H., Blichert-Toft, J., Hanan, B. B., Polve, M., Davies, G. R., et al. (2009). Geochemical stages at Jasper Seamount and the origin of intraplate volcanoes. *Geochemistry, Geophysics, Geosystems*, *10*, Q02001. https://doi.org/10.1029/2008GC002236

Kurz, M. D., Le Roex, A. P., & Dick, H. J. B. (1998). Isotope geochemistry of the oceanic mantle near Bouvet triple junction. *Geochimica et Cosmochimica Acta*, *62*, 841–852.

Kurz, M. D., Curtice, J., Lott, D. E., III, & Solow, A. (2004). Rapid helium isotopic variability in Mauna Kea shield lavas from the Hawaiian Scientific Drilling Project. *Geochemistry, Geophysics, Geosystems*, *5*, Q04G14. https://doi.org/10.1029/2002GC000439

Lekić, V., Cottaar, S., Dziewonski, A., & Romanowicz, B. (2012). Cluster analysis of global lower mantle tomography: A new class of structure and implications for chemical heterogeneity. *Earth and Planetary Science Letters*, *357–358*, 68–77.

Legendre, C., Maury, R. C., Caroff, M., Guillou, H., Cotton, J., Chauvel, C., et al. (2005). Origin of exceptionally abundant phonolites on Ua Pou Island (Marquesas, French Polynesia): Partial melting of basanites followed by crustal contamination. *Journal of Petrology*, *46*, 1925–1962.

Le Roex, A. P., Chevallier, L., Verwoerd, W. J., & Barends, R. (2012). Petrology and geochemistry of Marion and Prince Edward Islands, Southern Ocean: Magma chamber processes and source region characteristics. *Journal of Volcanology and Geothermal Research*, *223–224*, 11–28.

Lu, C., & Grand, S. P. (2016). The effect of subducting slabs in global shear wave tomography. *Geophysical Journal International*, *205*, 1074–1085.

Luais, B. (2004). Temporal changes in Nd isotopic compositions of Piton de la Fornaise magmatism (Réunion Island, Indian Ocean), *Geochemistry, Geophysics, Geosystems*, *5*, Q01008. https://doi.org/10.1029/2002GC000502

Lupton, J. E., Graham, D. W., Delaney, J. R., & Johnson, H. P. (1993). Helium isotope variation in Juan de Fuca basalts. *Geophysical Research Letters*, *20*, 1851–1854.

Macpherson, C., Hilton, D. R., Sinton, J. M., Poreda, R. J., & Craig, H. (1998). high $^{3}He/^{4}He$ ratios in the Manus backarc basin: implications for mantle mixing and the origin of plumes in the western Pacific Ocean. *Geology*, *26*, 1007–1010.

Marty, B., Pik, R., & Gezahegn, Y. (1996). Helium isotopic variations in Ethiopian plume lavas: Nature of magmatic sources and limit on lower mantle contribution. *Earth and Planetary Science Letters*, *144*, 223–237.

Mata, J., Kerrich, R., Macrae, N. D., & Wu, T.-W. (1998). Elemental and isotopic (Sr, Nd, and Pb) characteristics of Madeira Islands basalts: evidence for a composite HIMU-EM I plume fertilizing lithosphere. *Canadian Journal of Earth Sciences*, *35*, 980–997.

Mazza, S. E., Gazel, E., Bizimis, M., Moucha, R., Béguelin, P., Johnson, E. A., et al. (2019). Sampling the volatile-rich transition zone beneath Bermuda. *Nature*, *569*, 398–403.

Millet, M.-A., Doucelance, R., Baker, J. A., & Schiano, P. (2009). Reconsidering the origins of isotopic variations in ocean island basalts: Insights from fine-scale study of São Jorge Island, Azores archipelago. *Chemical Geology*, *265*, 289–302.

Moreira, M., & Allègre, C. (2004). Helium isotopes on the Macdonald seamount (Austral Chain): constraints on the origin of the superswell. *Comptes Rendus Geoscience*, *336*, 983–990.

Moreira, M., Kanzari, A., & Madureira, P. (2012). Helium and neon isotope in São Miguel Island basalts, Azores archipelago: New constraints on the "low ^{3}He/^{4}He" hotspot origin. *Chemical Geology*, *322–323*, 91–98.

Moreira, M., Staudacher, T., Sarda, P., Schilling, J.-G., & Allègre, C. J. (1995). A primitive plume neon component in MORB: The Shona ridge-anomaly, South Atlantic (51-52°S). *Earth and Planetary Science Letters*, *133*, 367–377.

Mortimer, N., Gans, P. B., Meffre, S., Martin, C. E., Seton, M., Williams, S., et al. (2018). Regional volcanism of Northern Zealandia: Post-Gondwana break-up magmatism on an extended, submerged continent. In S. Sensarma, B. C. Storey, G. Soc, & London (Eds.), Large igneous provinces from Gondwana and adjacent regions. Vol. 463 (pp. 199–226) Special Publications.

Mourão, C., Mata, J., Doucelance, R., Madeira, J., Millet, M.-A., & Moreira, M. A. (2012). Geochemical temporal evolution of Brava Island magmatism: constraints on the variability of Cape Verde mantle sources and on carbonatite-silicate magma link. *Chemical Geology*, *334*, 44–61.

Parnell-Turner, R., White, N., Henstock, T., Murton, B., Maclennan, J., & Jones, S. M. (2014). A continuous 55-million-year record of transient mantle plume activity beneath Iceland. *Nature Geoscience 7*, 914–919.

Nakamura, Y., & Tatsumoto, M. (1988). Pb, Nd, and Sr isotopic evidence for a multicomponent source for rocks of Cook-Austral Islands and heterogeneities of mantle plumes. *Geochimica et Cosmochimica Acta*, *52*, 2909–2924.

Nicolaysen, K. P., Frey, F. A., Mahoney, J. J., M Johnson, K. T., & Graham, D. W. (2007). Influence of the Amsterdam/St. Paul hot spot along the Southeast Indian Ridge between 77° and 88°E: correlations of Sr, Nd, Pb and He isotopic variations with ridge segmentation. *Geochemistry, Geophysics, Geosystems*, *8*, Q09007. https://doi.org/10.1029/2006GC001540

Parai, R., Mukhopadhyay, S., & Lassiter, J. (2009). New constraints on the HIMU mantle from neon and helium isotopic compositions of basalts from the Cook-Austral Islands. *Earth and Planetary Science Letters*, *277*, 253–261.

Parmelee, D. E. F., Kyle, P. R., Kurz, M. D., Marreo, S. M., & Phillips, F. M. (2015). A new Holocene eruptive history of Erebus volcano, Antarctica using cosmogenic ^{3}He and ^{36}Cl exposure ages. *Quaternary Geochronology*, *30*, 114–131.

Paul, D., White, W. M., & Blichert-Toft, J. (2005). Geochemistry of Mauritius and the origin of rejuvenescent volcanism on oceanic island volcanoes. *Geochemistry, Geophysics, Geosystems*, *6*, Q06007. https://doi.org/10.1029/2004GC000883

Peyve, A. A., & Skolotnev, S. G. (2014). Systematic variations in the composition of volcanic rocks in tectono-magmatic seamount chains in the Brazil Basin. *Geochemistry International*, *52*, 111–130.

Pik, R., Marty, B., & Hilton, D. R. (2006). How many mantle plumes in Africa? The geochemical point of view. *Chemical Geology*, *226*, 100–114.

Reid, M. R., & Graham, D. W. (1996). Resolving lithospheric and sub-lithospheric contributions to helium isotope variations in basalts from the southwestern US. *Earth and Planetary Science Letters*, *144*, 213–222.

Reisberg, L., Zindler, A., Marcantonio, F., White, W., Wyman, D., & Weaver, B. (1993). Os isotope systematics in ocean island basalts. *Earth and Planetary Science Letters*, *120*, 149–167.

Ribe, N. M., & Christensen, U. R. (1999). The dynamical origin of Hawaiian volcanism. *Earth and Planetary Science Letters*, *171*, 517–531.

Ritsema, J., van Heijst, H. J., Deuss, A., & Woodhouse, J. H. (2011). S40RTS: A degree-40 shear-velocity model for the mantle from new Rayleigh wave dispersion, teleseismic traveltimes, and normal-mode splitting function measurements. *Geophysical Journal International*, *184*, 1223–1236.

Roden, M. F., Trull, T., Hart, S. R., & Frey, F. A. (1994). New He, Nd, Pb and Sr isotopic constraints on the constitution of the Hawaiian plume: results from Koolau volcano. Oahu Hawaii, USA.*Geochimica et Cosmochimica Acta*, *58*, 1431–1440.

Rogers, N., Macdonald, R., Fitton, J. G., George, R., Smith, M., & Barreiro, B. (2000). Two mantle plumes beneath the East African rift system: Sr, Nd and Pb isotope evidence from Kenya Rift basalts. *Earth and Planetary Science Letters*, *176*, 387–400.

Sarda, P., Moreira, M., Staudacher, T., Schilling, J.-G., & Allègre, C. J. (2000). Rare gas systematics on the southernmost mid-Atlantic ridge: Constraints on the lower mantle and the DUPAL source. *Journal of Geophysical Research*, *105*, 5873–5996. https://doi.org/10.1029/1999JB900282

Scarsi, P., & Craig, H. (1996). Helium isotope ratios in Ethiopian Rift basalts. *Earth and Planetary Science Letters*, *144*, 505–516.

Schiano, P., Burton, K. W., Dupré, B., Birck, J.-L., Guille, G., & Allègre, C.-J. (2001). Correlated Os-Pb-Nd-Sr isotopes in the Austral-Cook chain basalts: the nature of mantle components in plume sources. *Earth and Planetary Science Letters*, *186*, 527–537.

Schilling, J. (1991). Fluxes and excess temperatures of mantle plumes inferred from their interaction with migrating mid-ocean ridges. *Nature*, *352*, 397–403.

Schilling, J.-G., Kingsley, R., Fontignie, D., Poreda, R., & Xue, S. (1999). Dispersion of the Jan Mayen and Iceland mantle plumes in the Arctic: a He-Pb-Nd-Sr isotope tracer study of basalts from the Kolbeinsey, Mohns, and Knipovich ridges. *Journal of Geophysical Research*, *104*, 10543–10569.

Schwindrofska, A., Hoernle, K., Hauff, F., Bogaard, P., Werner, R., & Garbe-Schönberg, D. (2016). Origin of enriched components in the South Atlantic: Evidence from 40 Ma geochemical zonation of the Discovery Seamounts. *Earth and Planetary Science Letters*, *441*, 167–177.

Simmons, N. A., A. M. Forte, L. Boschi, & Grand, S. P. (2010), GyPSuM: A joint tomographic model of mantle density and seismic wave speeds, *Journal of Geophysical Research*, *115*, B12310. https://doi.org/10.1029/2010JB007631

Sinton, J. M., Ford, L. L., Chappell, B., & McCulloch, M. T. (2003). Magma genesis and mantle heterogeneity in the Manus back-arc basin, Papua New Guinea. *Journal of Petrology*, *44*, 159–195.

Sleep, N. (1990). Hotspots and mantle plumes: Some phenomenology. *Journal of Geophysical Research*, *95*, 6715–6736.

Spaeth, A., Le Roex, A. P., & Duncan, R. A. (1996). The geochemistry of lavas from the Comores archipelago, Western Indian Ocean: Petrogenesis and mantle source region characteristics. *Journal of Petrology*, *37*, 961–991.

Starkey, N. A., Stuart, F. M., Ellam, R. M., Fitton, J. G., Basu, S., & Larsen, L. M. (2009). Helium isotopes in early Iceland plume picrites: Constraints on the composition of high ^{3}He/^{4}He mantle. *Earth and Planetary Science Letters*, *277*, 91–100.

Stecher, O., Carlson, R. W., & Gunnarsson, B. (1999). Torfajökull: A radiogenic end-member of the Iceland Pb-isotopic array. *Earth and Planetary Science Letters*, *165*, 117–127.

Steinberger, B., Nelson, P. L., Nelson, S. P. G., & Wang, W. (2019). Yellowstone plume conduit tilt caused by large-scale mantle flow. *Geochemistry, Geophysics, Geosystems*, *20*, 5896–5912. https://doi.org/10.1029/2019gc008490

Stroncik, N., Niedermann, S., Schnabel, E., & Erzinger, J. (2011). Determining the geochemical structure of the mantle from surface distribution patterns? Insights from Ne and He isotope and abundance ratios. AGU Fall Meet Abstr. V51B-2519.

Stroncik, N. A., Trumbull, R. B., Krienitz, M., Niedermann, S., Romer, R. L., Harris, C., & Day, J. M. D. (2017). Helium isotope evidence for a deep-seated mantle plume involved in South Atlantic breakup. *Geology*, *45*, 827–830.

Stuart, F. M., Lass-Evans, S., Fitton, J. G., & Ellam, R. M. (2003). High ^{3}He/^{4}He ratios in picritic basalts from Baffin Island and the role of a mixed reservoir in mantle plumes. *Nature*, *424*, 57–59.

Sun, S.-S. (1980). Lead isotopic study of young volcanic rocks from mid-ocean ridges, ocean islands and island arcs. *Philosophical Transactions of the Royal Society A*, *A297*, 409–445.

Takeshi, H., & Kaneoka, I. (1997). The uniform and low $^{3}He/^{4}He$ ratios of HIMU basalts as evidence for their origin as recycled materials. *Nature*, *390*, 273–276.

Taran, Y. A., Fischer, T. P., Cienfuegos, E., & Morales, P. (2002). Geochemistry of hydrothermal fluids from an intraplate ocean island: Everman volcano, Socorro Island, Mexico. *Chemical Geology*, *188*, 51–63.

Taras, B. D., & Hart, S. R. (1987). Geochemical evolution of the New England Seamount chains: isotopic and trace-element constraints, *Chemical Geology*, *64*, 35–54.

Thomas, L. E., Hawkesworth, C. J., Van Calsteren, P. W., Turner, S. P., & Rogers, R. W. (1999). Melt generation beneath ocean islands: A U-Th-Ra isotope study from Lanzarote in the Canary Islands. *Geochimica et Cosmochimica Acta*, *63*, 4081–4099.

Torsvik, T. H., Svensen, H. H., Steinberger, B., Royer, D. L., Jerram, D. A., Jones, M. T., & Domeier, M. (2020). Connecting the deep Earth and the atmosphere. In H. Marquardt, S. Cottaar, J. Konter, & M. Ballmer (Eds.), *Mantle convection and surface expressions,*. Washington, DC: AGU.

Trønnes, R. G., Planke, S., Sundvoll, B., & Imsland, P. (1999). Recent volcanic rocks from Jan Mayen: Low-degree melt fractions of enriched Northeast Atlantic mantle. *Journal of Geophysical Research*, *B104*, 7153–7168.

Valbracht, P. J., Staudacher, T., Malahoff, A., & Allègre, C. J. (1997). Noble gas systematics of deep rift zone glasses from Loihi Seamount, Hawaii. *Earth and Planetary Science Letters*, *150*, 399–411.

Vance, D., Stone, J. O. H., & O'Nions, R. K. (1989). He, Sr and Nd isotopes in xenoliths from Hawaii and other oceanic islands. *Earth and Planetary Science Letters*, *96*, 147–160.

Vanderkluysen, L., Mahoney, J. J., Koppers, A. A. P., Beier, C., Regelous, M., Gee, J. S., & Lonsdale, P. F. (2014). Louisville Seamount Chain: Petrogenetic process and geochemical evolution of the mantle source. *Geochemistry, Geophysics, Geosystems*, *15*, 2380–2400.

White, W. M., & Duncan, R. A. (1996). Geochemistry and geochronology of the Society Islands: New evidence for deep mantle recycling Earth process. In A. Basu, & S. R. Hart (Eds.), *Reading the Isotopic Code* (pp. 183–206). Washington, DC: American Geophysical Union.

White, W. M., & Hofmann, A. W. (1980). Sr and Nd isotope geochemistry of oceanic basalts and mantle evolution. *Nature*, *296*, 821–825.

Widom, E., Carlson, R. W., Gill, J. B., & Schmincke, H.-U. (1997). Th-Sr-Nd-Pb isotope and trace element evidence for the origin of the São Miguel, Azores: Enriched mantle source. *Chemical Geology*, *140*, 49–68.

Williams, C. D., Mukhopadhyay, S., Rudolph, M. L., & Romanowicz, B. (2019). Primitive mantle helium is sourced from seismically slow region in the lowermost mantle. *Geochemistry, Geophysics, Geosystems*, *20*, 4130–4145.